

MODELING THE ECOLOGY OF THE WĒKIU BUG'S MAUNA KEA  
ENVIRONMENT

A THESIS SUBMITTED TO THE GRADUATE DIVISION OF THE UNIVERSITY OF  
HAWAI'I IN PARTIAL FULFILLMENT OF THE REQUIREMENTS FOR THE  
DEGREE OF

MASTER OF SCIENCE

IN

METEOROLOGY

DECEMBER 2011

By: Leigh Anne Eaton

Thesis Committee:

Steven Businger, Chairperson  
Thomas A. Schroeder  
Shang-Ping Xie

We certify that we have read this thesis and the, in our opinion, it is satisfactory in scope and quality as a thesis for the degree of Master of Science in Meteorology.

THESIS COMMITTEE

---

Chairperson

---

---

## ACKNOWLEDGEMENTS

I would first and foremost like to thank Dr. Businger for all his guidance and patience throughout this project. Without his continuous support and encouragement, I don't know how I would have finished. I would also like to thank Drs. Schroeder and Xie for being vital parts of my thesis committee.

I would like to also thank Dr. Glen Liston for his permission to use SnowModel. Without SnowModel and his helpful comments, this project would have been utterly impossible!

Very special thanks go out to Jesse Eiben and Ryan Lyman. I would like to give my upmost gratitude towards Jesse for providing me with a world of knowledge about the Wēkiu Bug, and always being there with my questions about field I knew very little about, entomology. Without Ryan Lyman, this project would have been near impossible. I would like to thank Ryan for all his time and energy in obtaining the Davis weather station data, which is a trek in itself to get! Additionally, I would like to thank him for making the case study field experiment possible. Christopher Chambers and Matt Foster were also key participants in the case study field experiment. I would like to thank them for donating their time and energy, and helping collect snowdepth measurements.

Last but not least, I would also like to thank Sara Couto da Silva for her work that is being done on the climatology of the Mauna Kea summit. She provided me with some very helpful information about the climate of Mauna Kea.

## ABSTRACT

The goal of this research is to develop a better understanding of Wēkiu Bug distribution and population health, which are controlled by summit geology and meteorology. This research aims to develop a better understanding of the areas on the summit of Mauna Kea that are affected by deposition and erosion of snowpack and food deposits, and how the wind's direction and velocities are influenced by the variable terrain.

SnowModel, a spatially distributed snow-evolution model, is used to construct snowfall and bug fall accumulation maps of the summit. Eight weather stations connected to telescopes on the summit and four Davis weather stations located in various pu'us give the necessary meteorological variables needed to run SnowModel. Snowdepth observations taken after a passing storm are used to validate the model.

SnowModel, shows considerable skill in reproducing snowdepth patterns on the summit. Through modeling efforts, greatest snow accumulations are found on Pu'u Wēkiu and Pu'u Haukea. Similar results are found in bug fall accumulation patterns. Highest accumulations on Pu'u Haukea are on the outer southern and southeastern slopes. Prevailing wind direction is most critical for the distribution of snowfall and bug fall on Pu'u Wēkiu. Easterly winds produce maxima on the outer western slope and inner eastern slope of Pu'u Wēkiu. Westerly winds produce maxima on the inner western slope and the outer eastern slope.

Snowfall and bug fall accumulations are fairly well collocated with previous Wēkiu Bug trapping sites.

## TABLE OF CONTENTS

Acknowledgments .....	iii
Abstract.....	iv
List of Tables.....	vi
List of Figures.....	vi
Chapter 1: Introduction.....	1
1.1 Mauna Kea Geography and Climate.....	2
1.2 Mauna Kea Plant and Animal Life.....	6
Chapter 2: Data and Methods.....	9
2.1 Observational Data.....	9
2.2 A spatial distributed snow-evolution model.....	11
Chapter 3: Results.....	17
3.1 Wind speed and direction changes due to summit pu’us.....	17
3.2 Case Study – 11 January 2011.....	17
3.1 Yearly snowfall and bug fall accumulations.....	21
3.1.1 2008 snowfall and bug fall.....	22
3.1.2 2009 snowfall and bug fall.....	24
3.1.3 2008-2010 snowfall and bug fall.....	27
Chapter 4: Conclusions and Discussion.....	29
4.1 Distribution of snowfall and bug fall due to local winds.....	29
4.2 Discussion.....	31
4.3 Future Work.....	35
Tables.....	37
Figures.....	38
References.....	76

## LIST OF TABLES

<u>Table</u>	<u>Page</u>
1. Weather station locations, elevations, recording variables, and valid dates.....	37

## LIST OF FIGURES

<u>Figure</u>	
1. Photograph of Mauna Kea from the northeast.....	38
2. Geological make up and permafrost locations on the summit.....	39
3. Average daily temperature and daily precipitation (2008, 2009).....	40
4. Flow around a hill.....	41
5. Surface pressure distribution, perturbation velocity profile, surface shear stress perturbation.....	42
6. Photograph of Wēkiu Bug.....	43
7. Study Domain.....	44
8. Key features of the snow-transport model.....	45
9. Modeled wind speed.....	46
10. Modeled wind direction.....	47
11. IR-satellite image – 11 January 2011 0600 UTC.....	48
12. WV-satellite image – 11 January 2011 0600 UTC.....	49
13. IR-satellite image – 13 January 2011 1800UTC.....	50
14. Hourly average temperature and wind speeds for 8 January 2011 1000 UTC to 15 January 2011 0900 UTC.....	51
15. Windrose for 8 January 2011 1000 UTC to 15 January 2011 0900 UTC.....	52
16. Pictures of field experiment.....	53
17. Snowdepth output for 11 January 2011 0959 UTC.....	54
18. Pu’u Wēkiu snowdepth output for 11 January 2011 0959 UTC.....	55
19. Pu’u Hau’oki snowdepth output for 11 January 2011 0959 UTC.....	56
20. Mauna Kea yearly snowfall (2008, 2009, 2010).....	57
21. Windrose for all 2008 winds.....	58
22. Windrose for 2008 snow event days.....	59
23. Modeled snowdepth for 2008 (summit).....	60

24. Modeled snowdepth for 2008 (Pu’u Hauouki, Pu’u Pōhaku, Pu’u Poli’ahu, Pu’u Hau’oki, Pu’u Wēkiu).....	61
25. Modeled bug fall for 2008 (summit).....	62
26. Modeled bug fall for 2008 (Pu’u Hauouki, Pu’u Pōhaku, Pu’u Poli’ahu, Pu’u Hau’oki, Pu’u Wēkiu).....	63
27. Windrose for all 2009 winds.....	64
28. Windrose for 2009 snow event days.....	65
29. Modeled snowdepth for 2009 (summit).....	66
30. Modeled snow depth for 2008 (Pu’u Hauouki, Pu’u Pōhaku, Pu’u Poli’ahu, Pu’u Hau’oki, Pu’u Wēkiu).....	67
31. Modeled bug fall for 2009 (summit).....	68
32. Modeled bug fall for 2009 (Pu’u Hauouki, Pu’u Pōhaku, Pu’u Poli’ahu, Pu’u Hau’oki, Pu’u Wēkiu).....	69
33. Windrose for all 2010 winds.....	70
34. Modeled bug fall for 2010 (summit).....	71
35. Modeled snowfall for 2008-2009 (summit) with trap locations.....	72
36. Modeled bug fall for 2008-2010 (summit) with trap locations.....	73
37. Modeled snowfall for 2008-2009 (Pu’u Hauouki, Pu’u Pōhaku, Pu’u Poli’ahu, Pu’u Hau’oki, Pu’u Wēkiu).....	74
38. Modeled bug fall for 2008-2010 (Pu’u Hauouki, Pu’u Pōhaku, Pu’u Poli’ahu, Pu’u Hau’oki, Pu’u Wēkiu).....	75

# Chapter I: Introduction

The island of Hawai'i is flanked by two massive volcanoes, Mauna Kea and Mauna Loa, meaning “White Mountain” and “Long Mountain”, respectively (Fig. 1). Mauna Kea is the highest point in all of Pacific Polynesia, standing at 4,205 m. In ancient Hawaiian beliefs, the high elevation summits were considered to be sacred grounds, with Mauna Kea being the most sacred. In more current times, the summit of Mauna Kea is known for its premier ground-based astronomy.

Classified as a semi-arid, barren alpine desert tundra, the summit of Mauna Kea is cool to cold and extremely dry with nocturnal freezing temperatures throughout the year, and there is a very low-density of vascular plants (Ugolini, 1974). Summit temperatures, on average fluctuate between  $-5^{\circ}\text{C}$  and  $5^{\circ}\text{C}$  (da Silva, 2006). This barren alpine desert is topographically scattered with pu'us (cinder cones) that were created from explosions within the post-shield stage. The explosions produced highly vesicular material such as ash, lapilli, and cinder. The ash was carried downwind, and the lapilli and cinder fell close to the source, forming the massive cinder cones (Porter, 1997). There is evidence of glaciation that also helped to shape the summit's topography. Accumulation of boulders, stones, cinders, ash, and other debris, also known as moraines and tills, can be found on the slopes of Mauna Kea. Striations, steepened sides, and discoloration are very distinct on two pu'us, Poli'ahu and Wēkiu (USGS, 2007). Permafrost, ground that is permanently frozen for at least two years, is also evident on the summit. Eshes (2007) showed the north slopes and pu'u centers have the highest presence of permafrost (Fig. 2).

### *1.1 Mauna Kea Geography and Climate*

The Hawaiian Islands are situated in the middle of the Pacific Ocean, with Mauna Kea located  $\sim 20^{\circ}\text{N}$  and  $\sim 155^{\circ}\text{W}$ . Due to the Hadley circulation, there is a semi-permanent anticyclone at sea level over the northeastern Pacific Ocean. The southern branch of the Hadley cell is located  $\sim 10^{\circ}\text{N}$  and is associated with convergence and rising motion. At  $\sim 30^{\circ}\text{N}$  the descending branch of the Hadley cell is associated with subsidence and sinking motion. The location of the surface high is controlled by the sun's zenith point. The surface high creates northeasterly flow which is responsible for the low-level wind regime (the trade winds) that dominates Hawaiian weather and climatological patterns. The trade wind inversion in the Hawaiian Islands is present 82% of the time, with a mean base altitude of 2255 m and a mean thickness of 281 m (Cao et al., 2007). For a majority of the time, Mauna Kea's summit sits well above the trade wind inversion, which traps most cloudiness, water vapor, and pollutants within 1,500-3,000 m of sea level (Grindinger, 1992), giving the summit ideal conditions for star-gazing. The location and strength of the northeastern Pacific high, greatly influences the conditions on Mauna Kea.

There are two main seasons in the Hawaiian Islands, the warm season (Kau) and the cool season (Hoo-ilo), and can be represented by the location of the surface high pressure. The Pacific high, and with it the trade wind zone, moves north and south with sun and the highest occurrence of trades occurs between May and September. (Blumenstock and Price, 1967). During the Hawaiian cool season (October-April) the surface high pressure shifts southward, with its center  $\sim 30^{\circ}\text{N}$ ,  $130^{\circ}\text{W}$ . On Mauna Kea, Bely (1987) found the wind regime at the summit to be in trades 28% of the time during

the winter (October -April) and 57% during the summer (May - September). In the summer, the surface high pressure recedes northward and expands, with a center location of  $\sim 35^{\circ}\text{N}$ ,  $155^{\circ}\text{W}$ .

Various synoptic features can interrupt the trade wind regime. In the warm season, upper-tropospheric cold core lows, tropical cyclones, and TUTT cells can be present. The TUTT cell (tropical upper tropospheric trough) forms from a train of upper-tropospheric cold core lows. In the cool season, the Hawaiian Islands may be affected by extratropical cyclones, cold fronts, upper level lows, and Kona storms. These cool season storms can bring hazardous conditions, such as flash floods, heavy rains, high winds and surf, and even blizzards. On average, nine cold fronts pass over the Hawaii Islands during the winter season (Worthley, 1967). These passages bring the blizzard-like conditions to the taller summits (Haleakela, Mauan Loa, Mauna Kea). This is where Mauna Kea gets its name, from the winter time blanket that occurs with these synoptic disturbances.

Snow on the summit can occur during anytime of the year. In da Silva's (2006) study a snowfall proxy was created to establish an approximate average number of days with snow. For a snow event to be considered, the temperature and relative humidity must be below  $0^{\circ}\text{C}$  and greater than 80% for at least four hours. On average, January recorded the most snowfall events (six), February and March both averaged five, and November averaged four. El Niño brings drier conditions to the summit, while La Niña brings wetter than normal conditions (da Silva, 2006). The winter of 2008 was classified as a moderate La Niña, January and February 2008 recorded high amounts of precipitation (Fig. 3a). The 2009-2010 winter was an El Niño event, precipitation is significantly lighter than the 2008 La Niña and the 2008- 2009 neutral winter (Fig. 3b).

Bely (1987) and da Silva (2006) found mean wind speeds that were comparable with each other. Bely found, at the Canada France Hawaii Telescope (CFHT) the mean wind speed to be 6.69 m/s, while da Silva found the mean wind speed at CFHT to be 4.82 m/s, with a standard deviation of 1.49 m/s. The slight differences may be from length and years of data used, Bely focused on a single year (1983), and da Silva used a series between January 1994 and March 2006. In Bely's work, the University of Hawaii 2.2 meter telescope (UH), the Infrared Telescope Facility (IRTF), and radiosondes at 4200 meters from Hilo, Hawaii were examined for mean wind speeds. UH measured a mean speed of 6.17 m/s, IRTF a mean speed of 4.11 m/s, and the radiosondes a mean speed of 5.68 m/s. da Silva included the United Kingdom Infrared Telescope (UKIRT), which had a mean speed of 3.79 m/s. The altitude of IRTF, is comparably lesser than that of UH or CFHT. UKIRT's altitude is also slightly less than that of CFHT.

Consistent with the nature of shield volcanoes, the slopes of Mauna Kea are generally smooth and gradual (on average 7-12% grade). However, on the summit, slopes of 30% can be seen on the flanks of the various pu'us.

A majority of the flow above trade wind inversion is forced around Mauna Kea, the remaining flow is forced over the summit as a function of the froude number. The flow surrounding the pu'us on the summit is not generally a function of the froude number. The speed, direction, and turbulence associated with wind, all change as it flows over hills (Jackson and Hunt, 1975). Unstable and neutrally stable air is easily carried over a hill. For stable air, the degree of stability, the speed, and the terrain characteristic determine how the protruding hills or pu'u affect the flow. The more stable the air is, the more resistant it is to lifting and the greater likelihood that it will flow around a barrier

(Whiteman, 2000). Highest wind speeds from flow around a barrier are on the slopes where flow is parallel to the peaks contour lines (Fig. 4).

As the wind reaches the protruding pu'us and travels upslope, the stratified layers are compressed, and therefore produce faster velocities. On the leeside of the protrusions, the stratified layers are able to expand, and velocities decrease. Pressure in the layers is continuous and pressure perturbations exist from the variable terrain. Jackson and Hunt (1975) show that the perturbation pressure leading up to the peak of a hill increases, as does the perturbation velocity. The changes in normalized surface pressure distribution, normalized perturbation velocities, and normalized surface shear stress over a hill are shown in figures 5a-c. The greatest velocity and shear stress increases occur on the upper windward slope, close to the top of the hill. The greatest increase in velocity is seen close to the surface of the hill. On the lower leeward slope of the hill, velocity perturbations become negative. The shape, steepness, and height of the protrusions help determine the effects the topography will have on the wind.

The boundary layer over Mauna Kea is very thin. During the night, the summit's boundary layer can be exceptionally thin, allowing a significant portion of the summit to be in the free atmosphere, thus giving it excellent conditions for star gazing. When the winds are weak, radiative cooling stabilizes the atmosphere on the summit and suppresses turbulence. Stronger winds interacting with the terrain help govern the magnitude of turbulent eddies, the depth of the boundary layer, and the vertical wind speed profile (Erasmus, 1986). During the day, temperatures on Mauna Kea are controlled by the incoming solar radiation and the turbulent exchange of heat. The maximum temperature is generally seen around 2300 UTC (da Silva, 2006). The influence of the free

atmosphere, as seen in Erasmus (1986) and da Silva (2006) keep the night time temperature from exponentially decreasing throughout the night; the night's equilibrium temperature is reached within a few hours of sunset. Each pu'u is unique, and variations of boundary layer properties are seen at each site.

### *1.2 Mauna Kea Plant and Animal Life*

At first glance the summit of Mauna Kea looks like a barren desert; however, there is actually a very diverse habitat of plants and animals. Between the cracks and crevices of the volcanic rock, small plants can be found. Approximately twenty-five different lichen and twelve different moss communities are found on the summit (Group 70 International, 2000). Several of the lichens and moss communities studied are endemic to Hawaii, with a few being site specific to the summit of Mauna Kea. The lichens are most abundant on the north and west facing slopes, while the mosses are most abundant on the north-northeast and south-southwest facing slopes.

Plants are not the only species that find a home on Mauna Kea, the summit houses a multitude of arthropods (spiders, moths, mites, spring-tails, centipedes, true bugs). Summit life is considered to be supported by an aeolian ecosystem, a term first introduced by Swan (1963), which describes a habitat that is solely dependent of the transport of nutrients (biological fallout: organic debris, insects) by the wind.

The Wēkiu Bug (*Nysius Wēkiuicola*) is a true bug that is endemic to the summit of Mauna Kea (Fig. 6). The Wēkiu Bug is currently listed as a candidate on the Endangered and Threatened Species list, with a listing priority number of 8 (Fish and Wildlife Service, 2010). Future development of the summit, the extreme conditions it

lives in, and climate change are cited as cause for candidacy.

The Wēkiu Bug, first collected by F.G. Howarth, S.L. Montgomery, and W.P. Mull in 1980, was primarily categorized by Ashlock and Gagne (1983). This tiny (4.5-5.5 mm) flightless bug is a part of the hemipteran family, Lygaeidae, which contains predominately seed and planter eaters. The Wēkiu Bug, however, is a predator/scavenger that feeds on the aeolian fallout found in the summits substrate (Eiben and Rubinoff, 2010). Tephra ridges, slopes with lapilli, talus slopes, and highly fractured rock substrates are favored habitats for the Wēkiu Bug. The large interstitial spaces allow the Wēkiu bug to thermoregulate, protect itself from adverse conditions, and find moisture. Englund et al., (2002) found the highest concentration of Wēkiu bugs to be near the inner and outer rims of the alpine cinder cones and within 150 ft of the peak.

Eiben and Rubinoff (2010) and Ashlock and Gagne (1983), found that the Wēkiu Bug is able to withstand extreme temperature fluctuations. In field observations, the rock surfaces of Wēkiu Bug habitat were as high as 46°C during the day and as cold as -15°C at night. The Wēkiu Bug survives cold temperatures by basking in the sun during the day and hiding in an insulated ash layer at night, the Wēkiu Bug actively thermoregulates, essentially managing their presence in the micro-habitat rather than evolving physiologically to endure its extremes (Eiben and Rubinoff, 2010).

Motivation behind this research is to gain a better understanding of the Wēkiu Bug's distribution and population health, which are controlled by summit geology and meteorology. Previous work has shown the summit's geological make-up is pretty well understood (Wolfe et al., 1997). The goal of this research is to develop a better understanding of the areas affected by deposition and erosion of snowpack and food

deposits, and how the wind's directions and velocities are influenced by the variable terrain. The idea of using a snow transport model comes from the hypothesis that frozen and dead bug fall will move in a similar manner to frozen precipitation in the wind field. We hope to investigate the summit scale micro-meteorology through observations and modeling, focusing on moisture and food transport, and its relationship to the distribution of the Wēkiu Bug.

## Chapter II: Data and Methods

The Wēkiu Bug has been an area of research for several years (Ashcock and Gagne, 1983; Englund et al., 2002; Eiben and Rubinoff, 2010). This research aims to connect the entomological and geological studies with a micro-meteorological study of the summit. Both observations and modeling are used in hopes of gaining a better understanding of the endemic Wēkiu Bug's habitat.

Mauna Kea is the northern volcano on Hawaii Island, the summit rises 4205 m above sea level and sits at 19.817N and -155.467W (Fig. 7). Elevation in the region ranges from 3741.6 m to 4205 m. The gridded data used in the study comes from the United States Geological Survey (USGS) 1/3 arc-second National Elevation Dataset (NED) over Hawaii. The central southern region of the domain is the northern tip of the Mauna Kea Ice Age Natural Area Reserve, which holds the Mauna Kea Adz Quarry.

### *2.1 Observational Data*

The summit of Mauna Kea houses the world's largest observatory for optical, infrared, and submillimeter astronomy. Presently, there are thirteen active telescopes on the summit, several which support a basic weather station. Additionally, four Davis weather stations were installed in 2007 in low-lying areas within four different pu'us (Hau'oki, Kea, Wēkiu, and Pōhaku) under the supervision of the Wēkiu Bug Scientific Advisory Committee (WBSAC).

This study uses meteorological data from eight of the thirteen telescopes; i) Canada France Hawaii Telescope (CFHT); ii) Infrared Telescope Facility (IRTF); iii)

James Clark Maxwell Telescope (JCMT); iv) Submillimeter Array (SMA); v) Subaru Telescope (Subaru); vi) University of Hawaii 2.2 meter Telescope (UH88); vii) United Kingdom Infrared Telescope (UKIRT); and viii) Very Long Baseline Array (VLBA) (Fig. 7). Table 1 describes time frames and variables observed from each of the weather stations. The locations of some of the stations on their observatories add some variability to the anemometer recordings. The CFHT station is location in close proximity to structure of the telescope, causing slight blockage from northerly winds. The UH anemometer has a tendency to freeze over, limiting its quality of observation. The UKIRT station is location very close to the true summit has a record of recording the highest Mauna Kea summit winds.

The four Davis weather stations installed in 2007 record temperature ( $^{\circ}\text{C}$ ), relative humidity (%), wind speed ( $\text{m s}^{-1}$ ), wind direction (degrees), and precipitation (mm) (Table 1). The stations were installed under the WBSAC, to obtain meteorological measurements at strategic points on the summit. Before installation of the Davis weather stations, the only available data sets were from the telescope summit stations; the installation of the Davis stations makes meteorological data from summit depressions (pu'u crater floors and by the base of the pu'us) available. The four stations are located on the northwestern slope of Pu'u Hau'oki (MK-Hau'oki), in the western depression of Pu'u Wēkiu (MK-Wēkiu), on the northeast slope of Pu'u Kea (MK-Kea), and in the eastern depression of Pu'u Pōhaku (MK-Pōhaku) (Fig. 7). Stations were visited on a monthly schedule to download recorded data. Collection was limited due to the difficult accessibility of the stations. Lengthy periods of missing data are present in the sets due to adverse weather conditions, unknown mechanical problems, and one case of vandalism.

A first round of quality control was performed on the data from all twelve of the stations used before it was ingested into the model. Three criteria were looked at; i) the initial quality control looked for values that were acceptable for the given variable, ie. negative values for wind speed, wind direction (all directions were recorded on the 0-360° scale), relative humidity, and precipitation are not plausible; ii) if a given hour's recording significantly exceed (positively or negatively) the post and prior recording, that hour would be disregarded; iii) if a variable was found to be constant over a period of six hours, that section would be disregarded.

A field experiment took place on 11 January 2011 to record snowdepth after a cold front had blanketed the summit with snow. Snowdepth measurements were recorded manually with the use of rulers and yard sticks. Location coordinates were given by hand-held GPS devices. Snowdepths were measured in the corners and the center of a 2' x 2' square surrounding a given location. The average of the five points was taken to give the ~snowdepth at the given location to account for the differing rock sizes that scatter the summit.

## *2.2 A spatially distributed snow-evolution model*

SnowModel is a spatially distributed snow-evolution modeling system, which includes first order physics required to simulate snow evolution within each of the snow climates (i.e., ice, tundra, alpine/mountain, prairie, maritime, and ephemeral) (Liston and Elder, 2006). SnowModel was created under the notion that all snow climates possess spatial distribution and evolution characteristics and all experience a form of accumulation and erosion/ablation. SnowModel has been tested on a variety of snowy environments (ie., Colorado (Greene et al., 1999), Antarctica (Liston et al., 2000), Idaho

(Prasad et al., 2001), Alaska (Liston and Sturm, 2002)).

SnowModel is comprised of four sub-models, MicroMet, EnBal, SnowPack, and SnowTran-3D. MicroMet was developed by Liston and Sturm (2006b) to produce high resolution atmospheric forcings (air temperature, relative humidity, wind speed, wind direction, incoming solar radiation, incoming longwave radiation, surface pressure, and precipitation) required to run spatially distributed terrestrial models over a wide variety of landscapes using meteorological point data (from weather stations). Included in MicroMet is a three-step preprocessor that helps to identify and /or correct deficiencies found in the station data. The three-step preprocessor includes similar quality control techniques as mentioned above. In addition to the checks previously done, MicroMet completes time frames by filling missing days/hours with an undefined value (-9999) and interpolated missing data. It uses the Barnes objective analysis scheme (Barnes, 1973; Koch et al., 1983) to interpolate irregularly distributed meteorological data to a regularly spaced grid, with corrections based on known temperature-elevation, wind-topography, and solar radiation- topography relationships (Liston and Sturm, 2006a). (Detailed physics are provided in Liston and Elder, 2006a)

EnBal uses the near-surface atmospheric conditions produce by MicroMet to simulate surface skin temperature and energy and moisture fluxes. Surface latent and sensible heat fluxes and snowmelt calculations are made using the surface energy balance model,

$$(1 - \alpha)Q_{si} + Q_{li} + Q_{le} + Q_h + Q_e + Q_c = Q_m ,$$

where  $Q_{si}$ , is the solar radiation reaching the earth's surface,  $Q_{li}$  is the incoming longwave radiation,  $Q_{le}$  is the emitted longwave radiation,  $Q_h$  is the turbulent exchange of sensible

heat,  $Q_e$  is the turbulent exchange of latent heat,  $Q_c$  is the conductive energy transport,  $Q_m$  is the energy flux available for melt, and  $\alpha$  is the surface albedo (Liston and Elder, 2006b). For all of the terms found in the equation, surface temperature is left as the only unknown, and solved for. Surface temperatures greater than  $0^\circ\text{C}$  indicate there is energy available for melting. The energy flux available for melt,  $Q_m$ , is solved by setting surface temperature to zero (Liston and Elder, 2006b). (Detailed physics are provided in Liston and Elder, 2006b).

SnowPack is a simple, single-layer, snowpack evolution model that calculates snowpack changes in response to the precipitation and melt fluxes defined by MicroMet (Liston and Elder, 2006b). The compaction-based snow-density evolution is based on Anderson (1976). SnowPack uses snow temperature, overlying snow weight, and the effect of snow melting to calculate temporal snow-density changes. In the case of non-blowing snow, static-surface sublimation is calculated, and used to adjust the snow pack.

SnowTran-3D simulates wind-driven snow-depth evolution over topographically variable terrain (Liston et al., 1998). There are five primary components; i) the wind-flow forcing field; ii) the wind-shear stress on the surface; iii) the transport of snow by saltation and turbulent suspension (the dominate wind-transport modes); iv) the sublimation of saltating and suspended snow, and v) the accumulation and erosion of snow at the snow surface (Fig. 8). The required model inputs include, topography, vegetation, and spatially distributed temporally variant weather data (precipitation, wind speed, wind direction, air temperature, and relative humidity).

Physics behind SnowTran-3D are primarily based on a mass-balance equation that describes the temporal variation of snow depth at each point within the simulated domain.

Accumulation and erosion of snow depth at each point results from the following processes; i) changes in horizontal mass-transport rates of saltation,  $Q_{salt}$  ( $\text{kg m}^{-1} \text{ s}^{-1}$ ); ii) differences in horizontal mass-transport rates of turbulent suspended snow,  $Q_{turb}$  ( $\text{kg m}^{-1} \text{ s}^{-1}$ ); iii) sublimation of transported snow particles,  $Q_v$  ( $\text{kg m}^{-1} \text{ s}^{-1}$ ), and iv) the incoming rate of water equivalent precipitation,  $P$  ( $\text{m s}^{-1}$ ). The mass-balance equation is

$$\frac{d(\rho_s \delta)}{dt} = \rho_w P - \left( \frac{dQ_{salt}}{dx} + \frac{dQ_{turb}}{dx} + \frac{dQ_{salt}}{dy} + \frac{dQ_{turb}}{dy} \right) + Q_v,$$

where  $t$  (s) is time;  $x$  (m) and  $y$  (m) are the horizontal coordinates in the east-west and north-south directions; and  $\rho_s$  and  $\rho_w$  ( $\text{kg m}^{-3}$ ) are the snow and water densities. The mass-balance equation is solved at every time-step, for every grid cell and is coupled with neighboring cells through spatial derivatives (Liston and Sturm, 1998). (Detailed physics are provided in Liston and Sturm, 1998)

Saltation and suspension are the dominate processes for moving snow and the transport rate can be described by wind speed relationships. Sublimation of wind transported snow is a function of wind speed, air temperature, humidity, particle size, and solar radiation (Marsh, 1999). Blowing snow leads to snow redistribution, where considerable accumulations can be found on the leesides of ridges and topographic depressions. For snow to be blown, it must surpass the vegetation holding depth, which includes the height of various vegetation, surface boulders, and other features blocking the path. The shear stress on the surface,  $u_*$ , (formulated as friction velocity), produce by the wind, is the determining factor for transport. It is defined by,

$$u_* = u_r \frac{\kappa}{\ln\left(\frac{z_r}{z_0}\right)},$$

where  $u_r$  ( $\text{m s}^{-1}$ ) is the wind speed at reference height  $z_r$  (m),  $z_0$  (m) is the surface roughness length, and  $\kappa$  is von Karman's constant. The friction velocity of a given wind must exceed a threshold friction velocity value ( $u_{*t}$ ) for transport to begin. The threshold friction velocity is considered to be lower ( $u_{*t} = 0.07\text{-}0.25 \text{ m s}^{-1}$ ) for fresh, loose, dry snow and during snowfall and higher ( $u_{*t} = 0.25\text{-}1.0 \text{ m s}^{-1}$ ) for older, wind hardened, dense, and/or wet snow where inter-particle bonds and cohesion forces are strong (Kind, 1981).

Saltation is the transport of snow in periodic contact with and directly above the surface; transportation rate roughly increases linearly with friction velocity (Pomeroy and Gray, 1990). Saltation must be present in order to have turbulent-suspended snow particles (Liston and Sturm, 1998). Liston and Sturm (1998) showed that at higher frictional velocities, suspension is the dominating mode of transport over saltation. Lastly, snow accumulation and erosion can be effected by sublimation (loss of mass to the snow particle). During blowing snow events, the rate of sublimation is determined by the temperature and humidity gradients, and produces significant reductions in moisture on areas where snow is relocated (Schmidt, 1982).

For the process of modeling the bug fall on the summit of Mauna Kea, only Micromet and SnowTran-3D sub-models are used. For bug fall accumulation and ablation, the SnowPack and EnBal sub-models are turned off, to eliminate the processes of melting and density changes from energy inputs. Within the SnowTran-3D sub-model, the third blowing snow process, sublimation is ignored. This eliminates evaporation of the solid matter bug fall. Bug fall is unable to lose mass to the atmosphere. The phase changes that snow usually goes through, evaporation and melting, does not occur for the

solid matter bug fall. To imitate solid matter bug fall, temperature, relative humidity, and precipitation were set as constants at 0°C, 100%, and 0.2 mm hr<sup>-1</sup>. Ten bug fall locations around the perimeter of the study domain were ingested into the meteorological variable gridded fields created by MicroMet. The bug fall locations ran the constants listed above for the outlying summit areas to mimic incoming insects/bugs on the summit.

## Chapter III: Results

### *3.1 Wind speed and direction changes due to summit pu'us*

MicroMet was run to model the changes that occur to winds as they interact with the pu'u stippled summit. Cardinal and intercardinal (north, south, east, west, northeast, southeast, southwest, and northwest) wind fields of  $7 \text{ m s}^{-1}$  were initialized into MicroMet to display how the pu'us effect winds from a given direction (Figs. 9-10).

Pu'u Wēkiu in all eight directions altered the winds the greatest. Winds with easterly components have the greatest positive wind speed changes on the pu'u (Figs. 9b,e,f). The outer eastern slope of Pu'u Wēkiu for these three scenarios (east, northeast, southwest) increase wind speeds by  $\sim 20\%$ . For both direct west and east winds, Pu'u Wēkiu forced more winds south around the pu'u than north (Figs. 10b,d). Pu'u Hau'oki does not exhibit any great speed changes. On Pu'u Hau'oki approaching winds with a westerly component experience the greatest directional change compared to winds with an easterly component (Figs. 10d,g,h). Wind speed changes due to interaction with Pu'u Haukea are most recognizable from winds that have north and east components (Figs. 9a,b,e,f,h and 10a,b,e,f,h). Increase, however, is not as sharp as seen on Pu'u Wēkiu. For all three pu'us, the center depressions experience wind that is  $\sim 40\%$  slower than surrounding winds.

### *3.2 Case Study – 11 January 2011*

SnowModel in its entirety was run to encompass a January 2011 low that sent a cold front across Hawai'i. At 0600 UTC 11 January 2011 the front was situated over the island of Hawai'i (Fig. 11). Southeasterly winds are found leading the cold front and

northwesterly winds are found trailing the front; a typical wind pattern seen in cold fronts (Fig. 11). Low-level convergence are present (Fig. 11), as well as upper-level divergence (Fig. 12). Three days later another cold front impacted the islands. The second front is over the summit of Mauna Kea by 1800 UTC, 13 January 2011 (Fig. 13).

Temperatures at the summit prior to the arrival of the initial cold front follow a relatively strong diurnal pattern that is driven by insolation (Fig. 14a). Summit temperatures lose their strong diurnal cycle due to stronger than normal winds ( $\sim 15\text{-}35\text{ m s}^{-1}$ ) and cloud cover from the consecutive frontal passages. Daily averages are colder than normal,  $\sim 5^{\circ}\text{C}$  (Fig. 14b). The summit experienced very strong winds during the frontal periods, by 14 January 2011 the winds return to  $5\text{-}10\text{ m s}^{-1}$ . Wind directions between 1000 UTC 09 January 2011 and 0900 UTC 11 January 2011 are predominately westerly to southwesterly (Fig. 15).

Between 21:30 UTC 11 January and 0000 UTC 12 January 2011, a field experiment on the summit measured the fallen and drifted snow in Pu'u Wēkiu and Pu'u Hau'oki (Figs. 16a). The first front dropped  $\sim 15\text{ cm}$  of frozen precipitation on the summit (Fig. 16b). Snow drifts had accumulations up to  $60\text{ cm}$ . Summit temperature, relative humidity, wind speed and direction, and precipitation observations from January 2011 were used as input for SnowModel.

SnowModel, with its four subroutines (MicroMet, EnBal, SnowPack, SnowTran-3D) was run to assess the snowfall accumulation and ablation on the summit (Fig. 17). The prevailing wind direction over mountainous terrain is crucial for snow accumulation. The upwind side is where most snowfall will initially fall. In general, the deepest snowdepths from blown snow in mountainous areas are seen on the leeward side of ridge lines.

Wind speed determines the location of the greatest depth, the stronger the winds, the further downwind the area of greatest depth will be found. Scouring on ridges and windward sides is a common characteristic of drifting snow patterns. Top loading and cross loading are two methods of snow accumulation. Top loading occurs from wind blowing up a slope, and cross loading occurs from wind blowing across a slope.

The majority of the winds were westerly to southwesterly (Fig. 14). Output from SnowModel for 10 January 2011 covers a majority of the summit in ~15 cm of snow. This is in good agreement with observed depth. Pu'u Haukea, in the central southern region, showed strong scouring on the outer west slope of the pu'u, modeled depths were ~10 cm. On the inner western slope of Pu'u Haukea, maximum depths of ~33 cm are depicted. Pu'u Haukea has a generous depression in the center creating two windward and leeward slopes on the pu'u. Both the outer western slope and the inner eastern slope are considered windward slopes for this case study. The inner western and outer eastern slopes are considered to be leeward for the prevailing wind direction. On the eastern outer slope of Pu'u Haukea there is a shallower maximum of ~25 cm.

Similar wind-blown snow patterns are seen on Pu'u Wēkiu. Pu'u Wēkiu covers a substantially larger area than Pu'u Haukea, ~3x the size. The depths are approximately the same as Pu'u Haukea. Pu'u Hau'oki is northwest of Pu'u Wēkiu; the depression in the center of the pu'u is not as sharp or as deep as Pu'u Haukea or Pu'u Wēkiu. Scouring on the inner eastern slope of the pu'u is prevalent, as well as deposition on the outer eastern slope. The west side of Pu'u Poli'ahu is not as sharp and sloped as the previous pu'us. The west side is characterized by a mountainous area extending 500 m beyond the pu'u lip. Snowdrifts accumulate just east of the initial mountainous terrain, on the inner western

slope of the pu'u, and the outer eastern side. The drifts are not as deep as Pu'u Haukea or Pu'u Wēkiu. The first accumulation has the deepest snow, ~23 cm, and the second accumulations are ~20 cm.

Snowdepth measurements were recorded in Pu'u Wēkiu and Pu'u Hau'oki. The snowdepth measurements are plotted against model output at 0959 UTC 11 January 2011 (Figs. 18-19). The field experiment took place between 21:30 UTC 11 January and 0000 UTC 12 January 2011. The previous day was used for validation because the summit received more snowfall later in the day. Model output shows accumulation at 0959 UTC for each day, this is the end of day at 23:59 HST.

The overall spatial pattern of the model is in agreement with snowdepth observations. In the center of Pu'u Wēkiu (Fig. 18), both modeled and observed values display shallower snowdepths. The model has a tendency to overestimate in the center of the pu'u. The model and snowdepth observations are thicker towards the inner western slope of Pu'u Wēkiu. The model had a tendency to underestimate when observed snowdepths are particularly deep.

Within Pu'u Hau'oki (Fig. 19), the overall spatial pattern from the model and observations were in agreement. In the western crease of the pu'u center, the model did a fair job in representing snowdepths. The model underestimates the inner northern slope of the pu'u, but is in agreement with the increase in snowdepth that is occurring spatially; which also holds true for the inner western slope.

The overall spatial patterns from the model are in agreement with the observations. However, there is still a great deal of variability within the direct comparisons of snowdepths. Although, an average snowdepth value was recorded for

each observed location, the model's output resolution and 1/3 arc-second NED input, are not high enough resolution to resolve every boulder on the summit which causes variations across the snowdepth field.

### *3.3 Yearly snowfall and bug fall accumulations*

Yearly snowfall depth is modeled in the same manner as the case study. Meteorological input conditions from the available weather stations are interpolated over the study domain. The yearly snowfall output is the summation of the snowdepths (m) of days during the given year where precipitation received is  $\geq 0.3$  mm and temperature was  $\leq 0^{\circ}\text{C}$ . Only 2008 and 2009 are modeled due to the limited snowfall observations in 2010 (Fig. 20).

Yearly bug fall accumulation is created using summit winds (including speed and direction) from 2008 to 2010. SnowModel was run to simulate bug fall patterns on the summit. EnBal and SnowPack subroutines were not incorporated into simulated bug fall events, to eliminate the processes of melting and density changes from energy inputs. A snow transport model was used to model the bug fall distribution on the summit under the assumption that dead or frozen bugs arriving at the summit will move in a similar way as frozen precipitation. It was assumed that bugs that fall on the windward sides of pu'us would tend to be blown to the leeward sides by the terrain forced variations in the winds.

Solid bug fall matter in the atmosphere was imitated by convincing the model that solid precipitation was falling. This was done by forcing the air temperature and relative humidity to be constants at  $0^{\circ}\text{C}$  and 100%, and precipitation to be a constant falling at a rate of  $0.2 \text{ mm hr}^{-1}$ . There are not enough data available regarding actual bug fall to

quantitatively assign a rate of incoming bug matter per hour of the day. The precipitation rate is arbitrarily set to allow for clear patterns of bug fall accumulation in the model output. The hypothetical accumulation scale (non-dimensional) was created using modeled bug fall depth output, where zero on the scale is equivalent to the lowest predicted output depth and five is equivalent to the highest predicted output depth.

### *3.3.1 2008 snowfall and bug fall*

The summit experiences winds with easterly components 64% of the time in 2008, with total summit winds being greater than  $10 \text{ m s}^{-1}$  18% of the time (Fig. 21). Northeasterly and southeasterly winds are greater than  $10 \text{ m s}^{-1}$  21% and 20% of the time. Easterly winds prevail in snow events for 2008, especially in February, March, and November (Figs 22a-b). December snow events are governed by both easterly and westerly winds, the same goes for snow events in April.

The summit received snowfall 40 days out of the year for 2008. Total average snowfall observed for the year was 193 mm. Model output shows areas, specifically the outer southern and inner eastern slopes of the pu'us, where snowfall accumulations are the greatest for the entire year (Fig. 23). Over the year period, the model shows these slopes with yearly accumulations up to 9 m. The southeastern portion of the domain accumulates an order of magnitude more snowfall than the northwestern portion. Similar accumulation variations are seen between the northwestern portion of the domain and the southeastern portion. The more dominant easterly winds are a big factor in this snowfall distribution.

The outer northern slope of Pu'u Haukea is susceptible to scouring under the

winds observed during snow events in 2008 (Fig. 24a). Snowdepths on this slope are between 2 to 3m. The southern outer slope of Pu'u Haukea accumulates ~2.5 times more snow than the northern outer slope; accumulations for the year are between 5 to 7 m. The inner northern slope of Pu'u Haukea accumulates similar amounts of snowfall on the outer southern slope.

Pu'u Hau'oki displays similar snowfall patterns as Pu'u Haukea (Fig. 24b). The southern outer slope of Pu'u Hau'oki accumulates ~6 m of snowfall. Heavy scouring is evident on the northern outer slope. The highest snowfall accumulation on the summit for 2008 occurs on the eastern inner slope of Pu'u Wēkiu. Maxima values are upwards of 9 m. The eastern outer slopes of Pu'u Wēkiu and the ridge extending north from the pu'u are characterized by strong scouring, especially in the troughing region just north of Pu'u Wēkiu. Much like the inner base of Pu'u Haukea, there is minimal accumulation in Pu'u Wēkiu's inner base. Accumulations of 7 to 8 m occur on the outer southern and southwestern slopes of Pu'u Wēkiu, as well as the west side of the ridge extending north from Pu'u Wēkiu.

Snowfall maxima occur on the southern slopes of the heart-shaped Pu'u Poli'ahu and Pu'u Pōhaku (Fig. 24c). Accumulations on the Pu'u Pōhaku are 1 to 2 m shallower than the 6 to 7 m accumulations on Pu'u Poli'ahu. The outer southwestern slope of Pu'u Poli'ahu is made up of a variety of lateral ridges. Large snowfall deposits occur on the southwest slopes.

Areas of high accumulations of bug fall on the summit agree with areas of greatest snowfall accumulations (Fig. 25). Bug fall accumulation maxima on Pu'u Haukea occur on the outer southern slope much like the snowfall (Fig. 26a). However, two bug fall

maxima occur on the southeastern and southwestern slope instead of a lateral on Pu'u Haukea. Total winds for 2008 have a much stronger northeasterly influence than the snow event winds, which can account for the additional maxima. Additionally, the inner northern slope maximum does not occur for modeled bug fall density.

Bug fall on Pu'u Hau'oki is very minimal, with light accumulation occurring on the outer southern slope (Fig. 26b). The bug fall accumulation is not as prominent on Pu'u Hau'oki as is the snowfall. Pu'u Wēkiu, on the other hand, experiences bug fall accumulations much like the snowfall (Fig. 26b). The overall bug fall density maximum occurs on the inner eastern slope of Pu'u Wēkiu. Similar bug fall accumulation increases also occur on the west side of the ridge extending north from Pu'u Wēkiu and the outer southern and southwestern slopes of Pu'u Wēkiu.

The maxima bug fall accumulations on Pu'u Pōhaku for 2008 is on the outer western slope (Fig. 26c). Snowfall maxima occur on the southern slope of the pu'u. The dominant easterly winds during snow events allow for cross loading to occur on the outer southern slope of Pu'u Pōhaku . Pu'u Poli'ahu does display bugfall maxima on the southern slope. Bug fall maxima do not occur in the lateral ridges on the southwestern slope of Pu'u Poli'ahu.

### *3.3.2 2009 snowfall and bug fall*

Summit winds during 2009 are nearly evenly split between easterly and westerly flow (Fig. 27). Winds with a northwesterly component are greater than  $10 \text{ m s}^{-1}$  27% of the time, and winds with a southwesterly component are greater than  $10 \text{ m s}^{-1}$  28% of the time. Both northeasterly and southeasterly wind percentages that are greater than  $10 \text{ m s}^{-1}$

are significantly smaller. Winds during snow events for 2009 are predominantly westerly (Fig. 28a-b). January, March, and November have the greatest variation in snow event wind direction. In November there are a number of events with average winds being northerly. In January and March there are a number of snow events having easterly winds. The higher percentages of northeasterly and southeasterly winds are not seen during snow events. Winds with strong northern and southern influences are also less frequent during snow events.

Snowfall on the summit was recorded during 52 days out of the year for 2009, and the annual average amount is 239 mm. Yearly summed accumulations in some areas exceed 9 m. The upper northwest and the lower southwest portions of the domain have the lowest accumulations of snowfall (Fig. 29), which differs from 2008, reflecting the different wind pattern. The southern and southeastern slopes and the outer eastern slopes have the deepest snowfall accumulations.

Snowfall maxima surrounding Pu'u Haukea occur strongly on the outer southern and eastern slopes, with accumulations between 8 and 9 m (Fig. 30a). The inner northwestern slope accumulates ~7 m. Strong scouring results in minimal snow cover on the northwestern slope.

The outer southeastern slope of Pu'u Hau'oki accumulates between 8 and 9 m of snowfall during 2009 (Fig. 30b). Similar to Pu'u Haukea, the center depression is clear of deep snowfall accumulations and a maximum occurs on the inner northwestern slope. Pu'u Wēkiu and the ridge extending north off of the pu'u experience the highest snowfall accumulations on the summit for 2009 (Fig. 30b). The outer eastern slope of Pu'u Wēkiu holds depth values beyond 9 m, as well as the eastern slope of the extending ridge. High

snowfall accumulation, 8 to 9 m, occurs on the inner western slope of Pu'u Wēkiu. The minimum snowfall accumulation in the center depression of Pu'u Wēkiu is not as minimal as seen in 2008.

Pu'u Pōhaku and Pu'u Poli'ahu experience similar snowfall deposition patterns in 2008 and 2009 (Fig. 30c). Moderate snowfall accumulation, 4 to 5 m, occurs on the southern slope of Pu'u Pōhaku. The snowfall maximum on Pu'u Poli'ahu occurs on the southern slope. Part of this snowfall maximum extends to the eastern outer slope of the pu'u, this feature is not seen in 2008. The lateral ridge maxima on the southwest slope are also present in 2009.

Overall the bug fall and the snowfall distributions agree. Bug fall maxima occur on the eastern outer and southern slopes (Fig.31). Bug fall accumulations on the outer eastern slope of Pu'u Haukea exceed the maximum value (Fig. 32a). Other areas of high bug fall accumulation on the pu'u are the outer southern slope and the inner western slope. These two areas agree with the snowfall patterns and depths seen for 2009.

Pu'u Wēkiu bug fall accumulations are the highest on the eastern outer slope (Fig. 32b). Maximum snowfall is collocated with this result. This holds true from the maximum bug fall accumulations occurring on the eastern side of the ridge extending northward from Pu'u Wēkiu. Strong scouring is present on the outer western slopes. The same discrepancy between bug fall and snowfall seen in 2008 surrounding Pu'u Hau'oki is also seen in 2009 (Fig. 32b). The high accumulation of snowfall for 2009 on the outer southwest slope of Pu'u Hau'oki is a result of cross loading from stronger northeast winds. Bug fall accumulation does not exceed ~3 for the southern slope of Pu'u Hau'oki. Scouring on the northwest slope is present.

Pu'u Pōhaku bug fall accumulation on the southern slope is light, under  $\sim 3$ , and has a similar pattern to the snowfall (Fig. 32c). Locations of bug fall accumulation occur on the southern slope, on the eastern slope, and between the southwestern lateral ridges (Fig. 32c). Snowfall accumulation locations have the same spatial distribution.

### *3.3.3 2008-2010 Snowfall and bug fall*

Summit winds of 2010 have similar characteristics as winds during 2008; the strongest winds are from the east and occur more frequently (Fig. 33). Summit winds during 2010 are greater than  $10 \text{ m s}^{-1}$  29% of the time. Bug fall patterns between 2008 and 2010 are spatially alike (Figs. 25, 34). Larger accumulations of bug fall are a result of the higher occurrence of stronger winds in 2010. Under the assumption that 2008 and 2010 winds spatially distribute bug fall in a similar manner, it may be assumed that snowfall would be too. In this section, snowfall summation from 2008 to 2009 will be compared against the bug fall summation for 2008, 2009, and 2010, to provide an understanding of areas most conducive to Wēkiu Bug inhabitation. The 2-year total snowfall and the 3-year total bug fall patterns agree well with each other and for the most part the patterns for individual years also agree (Figs. 35,37). For the 2-year total and for the individual years, Pu'u Haukea's maxima for bug fall and snowfall occur on the outer southern and southeastern slopes (Figs. 36a,38a). A second snowfall maximum on the inner northeastern slope of Pu'u Haukea is seen. Pu'us Poli'ahu and Pōhaku also display similar patterns over the 2 and 3- year totals compared to the individual years for snowfall and bug fall (Figs. 36b, 38b). Maxima are still seen on the southern slopes of Pu'u Pōhaku and Pu'u Poli'ahu. The maxima associated with the lateral ridges on the

southwest slope of Pu'u Poli'ahu are well defined. Pu'u Wēkiu and Pu'u Hau'oki exhibit the greatest differences between the years (Figs. 36c, 38c). The 2 and 3-year totals clearly shows the affect wind direction and speed has on Pu'u Wēkiu, the largest pu'u in this study. Maxima on Pu'u Wēkiu are seen on both the inner and outer eastern slope and on either side of the ridge extending north from the pu'u. The higher values on the eastern slopes are the product of the higher wind speeds observed in 2009.

## Chapter IV: Conclusions and Discussion

The cinder cone (pu'u) stippled summit affects local wind patterns and summit deposition of moisture and nutrients. The pu'us can protrude as much as 200 m beyond their surrounding surface elevations. Surface wind speed and direction are altered by the variable terrain. In general, winds on the up-slope side of hills or pu'us and on the ridge are faster than those over flat terrain. On the down-slope sides, winds speeds tend to decelerate. As the wind approaches the pu'us, its direction is affected by the elevated terrain. It is either forced around or over the pu'u. Consequently, highest levels of snowfall and bug fall are seen on the leesides of ridges and crests. For the summit of Mauna Kea it was shown that winds with an easterly or northerly direction receive the greatest wind speed increase, especially on Pu'u Wēkiu. Depending on the concavity or convexity of the pu'u, wind direction can change as much as  $\sim 10^\circ$  as it's forced around the pu'u.

Understanding the spatial patterns of the snowfall and bug fall due to changes in wind as it interacts with the summit pu'us is of great interest in understanding the life, habitat, and distribution of the Wēkiu Bug.

### *4.1 Distribution of snowfall and bug fall due to local winds*

In this study it is assumed that the maximum bug fall accumulation patterns are governed by similar physics as snow transport. Highest levels of bug fall are seen on the leeward sides of the pu'us and the position of maximum accumulation is controlled by

wind strength. Scouring and lower accumulation areas are seen on the windward sides in high velocity scenarios. Differences in maxima accumulations occur between 2008, 2009, and 2010. Dominant wind direction is from the east in both 2008 and 2010, and for 2009 the dominant wind direction is from the west.

-Nutrient and moisture supplies on Pu'u Haukea are the greatest on the outer southern and southeastern slopes and the inner northwestern slope. This holds for 2008, 2009, and 2-year total. Stronger westerly winds in 2009 create more deposition of bug fall on the outer eastern slope than seen in other years.

-Pu'u Pōhaku's maxima of nutrients and moisture occur on the outer southern slope. There is a second bug fall maxima on the western slope. These patterns are found for both 2008, 2009, and the 2 and 3-year totals.

- Maximum moisture on Pu'u Poli'ahu is found continuously down the outer southern slope. Nutrient accumulation occurs mainly on the upper section of the outer southern slope. Down the inner northern slope, nutrient and moisture maxima occur in repeating patterns over the given years.

-Nutrient accumulation on Pu'u Hau'oki is minimal, moisture accumulation occurs strongly on the outer southern slope for 2008, 2009, and the 2-year total.

-Moisture and nutrient accumulation on Pu'u Wēkiu and the ridge line extending north from the pu'u vary greatly between the years from differing prevailing winds. Prevailing easterlies, like those in 2008 and 2010, have maxima moisture and nutrient accumulations on the inner eastern slope of Pu'u Wēkiu, the outer western slope on Pu'u Wēkiu and the ridge extending north from the pu'u. Highest nutrient concentrations are towards the upper portion of the slope. Stronger winds cause nutrients to also accumulate

on the outer northwestern slope of Pu'u Wēkiu.

-Prevailing westerlies, like those in 2009, allow for moisture and nutrients to collect along the inner western slope of Pu'u Wēkiu. Moisture and nutrient accumulation is the greatest on the outer eastern slope of Pu'u Wēkiu. Highest nutrient accumulations occur half way up the outer eastern slope. The eastern slope of the ridge extending from Pu'u Wēkiu traps nutrients on the upper portion of the slope.

#### *4.2 Discussion*

The synoptic scale winds on the summit are mainly controlled by the prevailing surface high pressure center that is located north of the Hawaiian Islands. On the local scale the variable terrain of the surface alters the wind significantly. The summit is an Aeolian system, where nutrients primarily come from matter being blown in. Areas of deposits differ with changing wind speeds and directions. The synoptic wind rotation from prevailing easterlies to prevailing westerlies affects accumulation patterns on the summit, with the greatest differences occurring on Pu'u Wēkiu. Western wind regimes deposit most nutrients on the outer eastern slopes of the pu'u, whereas, during easterly wind regimes the outer western and the inner eastern slopes of Pu'u Wēkiu accumulate the most nutrients. The strength of the wind greatly determines how much will be able to be carried. In comparing similar directional wind regimes (2008, 2010), snowfall and bug fall maxima accumulations occur further downslope in 2010 when winds are stronger. Increases in wind speed allows for increases in horizontal momentum, resulting in a further downslope location of moisture and nutrient deposition. Slope angle and aspect seems to have an effect on the accumulations, for both moisture and nutrient. For

instance, areas of lesser bug fall accumulations occurred in Pu'u Hau'oki and Pu'u Pōhaku compared to the very steep Pu'u Haukea and Pu'u Wēkiu.

Patterns of nutrients and moisture follow the previously known concepts regarding drifting and blowing snow. Bug fall and snowfall fields are not exact replicas due to the different set of winds used. The bug fall accumulations were modeled using winds from the entire year. For snowfall, only the winds that were present during snow events were used to distribute snowfall on the summit.

Sublimation is ignored when modeling bug fall; there are no losses to the maxima accumulations through phase changes. Nutrient maxima occur in clumped areas, while snowfall areas are more continuous down the slope. This clumping of maxima bug fall areas may arise from the constant temperature and humidity throughout the study period. Threshold friction velocity not only depends on wind speed, but also depends on temperature and the strength of the bond at the surface. Without evolving air temperature from 0°C, the simulated bug fall were cohesively strong and the change in friction velocities were limited to differences in wind speeds. The bug fall trajectory, through the study period, may have been more similar to each other from limited change in friction velocity.

During the cool season, winds have a dominant westerly direction and during the warm season winds have a dominant easterly direction. These patterns, however, can be altered under different ENSO regimes. Climatological records from da Silva's (2011) study show winds at the summit to be northeast to southeast 35% of the time and northwest to southwest 20% of the time. Under El Nino, da Silva (2011) found that westerly winds prevail, with northwest to southwest winds being present 46% of the time.

In La Nina conditions, the frequency of easterly winds increases from the climatological value by 5%. Northeast to southeast winds are present on the summit 40% of the time during La Nina. In this study, hints of these phases could be seen in the yearly runs. The beginning of the 2009-2010 winter (November, December) the summit winds are predominantly westerly. This winter was under a weak El Nino. The winter of 2010-2011 was under a weak La Nina, and summit winds had a more easterly component. The wind changes are most influential on Pu'u Wēkiu.

Several studies have helped determine the favorable locations for Wēkiu Bugs through various trapping techniques (Brenner, 2006; Englund et al., 2002; Englund et al., 2009; Eiben and Rubinoff, 2010). Wēkiu Bugs have been recorded on the west and northwest rim of Pu'u Haukea, in the flatter area between Pu'u Haukea and Pu'u Poli'ahu, on the northern side of Pu'u Hau'oki and on the southern and eastern rim, on the outer western slope of Pu'u Wēkiu, in the Pu'u Wēkiu center depression, on the inner eastern slope of Pu'u Wēkiu, and on the outer eastern slope of Pu'u Wēkiu and the ridge extending from the pu'u (Figs. 35-36).

Annual Wēkiu Bug field experiments led by Brenner (2006) from 2002 to 2006, find the highest count of Wēkiu Bugs in the spring. Brenner's (2006) field experiments were conducted on Pu'u Hau'oki and Pu'u Wēkiu. The most sampling has been done on Pu'us Hau'oki, Haukea, and Wēkiu. Englund et al. (2009) sampled a pu'u around VLBA in both 2007 and 2008. The north side of the pu'u only positively observed one Wēkiu Bug between 2007 and 2008. The south side positively observed eleven and nine Wēkiu Bugs in 2007 and 2008. The sample sites on Pu'us Hau'oki, Haukea, Wēkiu had considerably more Wēkiu Bug activity than the pu'u by VLBA. Englund et al. (2009)

compiled Wēkiu Bug sample site data from 2001 to 2008 showing that 822 Wēkiu Bugs have been seen observed on Pu'u Haukea over that 9-year period.

Englund et al. (2009) observed 537 Wekiu Bugs using 42 traps located on Pu'u Haukea, Pu'u Hau'oki, Pu'u Wekiu, and surrounding the pu'u by VLBA in 2007. The traps for 2007 had a total trap day number of 252. In 2008, their observations of Wekiu Bugs were ~7x less than observed in 2007. In 2008, 30 traps in ~the same summit locations counted 70 Wekiu Bugs. The 2008 study has a total trap day value of 120. The conditions during this field experiment are unknown, as well as how climate variation affects the summit, including its, temperature, moisture, winds, and the overall habitat of the Wekiu Bug.

All locations of Wēkiu Bug recordings, except for the area between Pu'u Haukea and Pu'u Poli'ahu and the center depression of Pu'u Wēkiu, receive high amounts of snow drift over the winter season. The locations that receive high snow drifts also accumulate the highest density bug fall, except for Pu'u Hau'oki. Bug fall accumulation is considerably less on Pu'u Hau'oki than Pu'u Haukea or Pu'u Wēkiu.

The pu'us are cinder cones and are made up of ash, lapilli, and cinder from explosions that occurred on the summit. This combination of volcanic rock allows for large interspatial areas between rocks to occur, a necessity for the Wēkiu Bug. A majority of the land surrounding the pu'us is comprised of older Hawaiiite-Mugearite lava flows, which is primarily made up of Laupāhoehoe 'a'ā lava with large rough sections. Surrounding Pu'u Pōhaku's base, the geological make up is primarily glacial till, as well as the eastern side of Pu'u Wēkiu. The finer make up of glacial till is unsuitable for Wēkiu Bug life.

Wēkiu Bug sample sites, areas of high moisture and nutrient accumulation, and areas with high interstitial spaces are found to be relatively well collocated. The locations of Wēkiu Bug sample sites do not interfere with areas made up of glacial till or permafrost. This may give more insight into the life and habitat of the endemic Wēkiu Bug.

Lichens are most commonly found on the north and west facing slopes of the various pu'us, and mosses are typically found on the outer north and northeast slopes and the outer south and southwest slopes (Group 70 International, 2000). Modeled bug fall and snowfall outputs show that accumulations are predominantly on the outer southern slopes and the outer northeast to southeast slopes. The locations of lichens and mosses fit well with the distribution of moisture. Lichens are poikilohydric, meaning they are able to survive on limited water supply. The northern and western slopes were found to accumulate low levels of snowfall. As for mosses, the southern slopes repeatedly saw high levels of snowfall. The outer northeast and southwest slopes of Pu'u Wēkiu also had high amounts of snowfall accumulation.

#### *4.3 Future Work*

Additional case studies of summit snowfall and drift will help further validate the model. Data assimilation of multiple days of snowdepth observations can be input into SnowModel to correct deficiencies in modeled snowdepth output. The availability of water from the summit is critical for understating the hydrological cycle of the mountain. Continuous work with SnowModel will give the ability to quantitatively assess the loss of moisture due to sublimation.

The availability of bug fall data is limited for this study. Ongoing entomological studies should be able to provide a more quantitative outlook on incoming bug fall.

With ongoing studies of the summit, more comprehensive studies of ENSO phases will help to map out more distinctive bug fall and snowdepth patterns for those years. Both future and previous records will help to assess ENSO impacts. Updated topography from recent and future construction projects could be included to determine how the changes to the land affect the distribution of moisture and nutrients on the summit. Inclusion of high resolution WRF winds into the SnowModel will help to forecast drifting snow conditions on the summit for winter storms.

**Tables:**

**TABLE 1**

Station	Lat (N)	Long. (W)	Elev. (m)	T (°C)	RH (%)	WS (m/s)	WD (°)	Precip. (mm/hr)	Valid Dates
MK -Hau'oki	19.8267	-155.4753	4138	X	X	X	X	X	01/2008 – 03/2009 05/2009 – 07/2009 10/2009 - 7/2010
MK-Wekiu	19.8192	-155.4697	4153	X	X	X	X	X	01/2008 04/2008 – 04/2009 09/2009 -03/2010 05/2010- 07/2010
MK-Kea	19.8261	-155.4683	4168	X	X	X	X	X	01/2008 – 01/2009
MK-Pohaku	19.8253	-155.4900	4003	X	X	X	X	X	01/2008 – 04/2008
UH88	19.8230	-155.4694	4214	X	X	X	X	X	01/2008 – 01/2011
CFHT	19.8253	-155.4688	4204	X	X	X	X		01/2008 – 07/2009 09/2009 – 01/2011
JCMT	19.8228	-155.4770	4075	X	X	X	X		05/3008 – 01/2011
UKIRT	19.8224	-155.4703	4199	X	X	X	X		01/2008 – 01/2011
SUBARU	19.8255	-155.4760	4163	X	X	X	X	X	01/2008 – 02/2008 05/2008 – 01/2011
VLBA	19.8014	-155.4555	4077	X	X	X	X	X	01/2008 – 01/2011
IRTF	19.8262	-155.4720	4168	X	X	X	X		01/2008 – 01/2011
SMA	19.8242	-155.4782	4080	X	X	X	X	X	01/2008 – 03/2008 05/2008 – 12/2008 07/2010 – 01/2011

Table 1: Weather stations and their locations, elevations, recorded variables, and valid dates.

**Figures:**



Fig. 1: Photograph of Mauna Kea from the northeast. Mauna Loa is visible in the background. (Picture by R. Wainscoat)

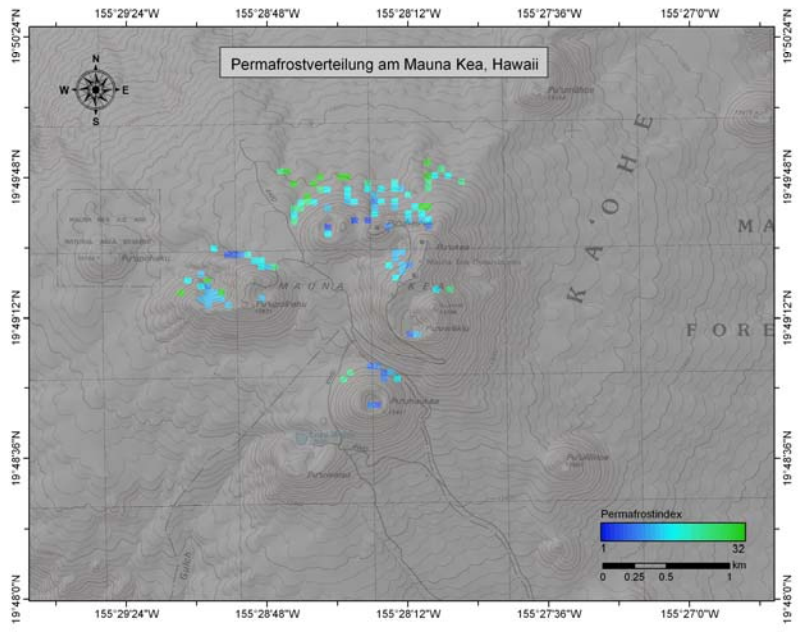
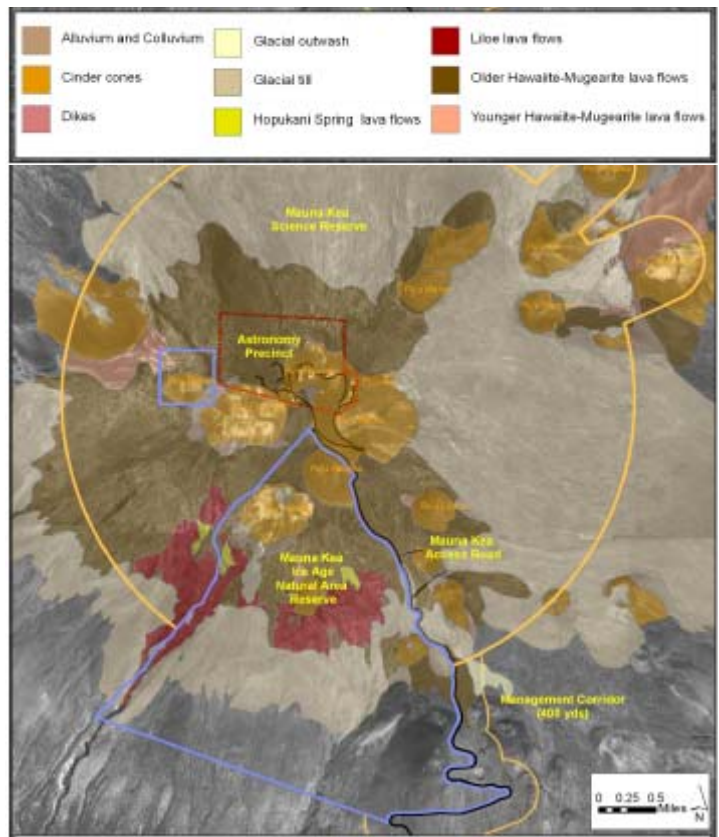


Fig. 2: a) Mauna Kea summit geological make up (Sustainable Resources Group International, Inc., 2009); b) Locations of possible permafrost on the summit of Mauna Kea. Permafrost index: Blue lower possibility, Green higher possibility. Figure from Ehses (2007).

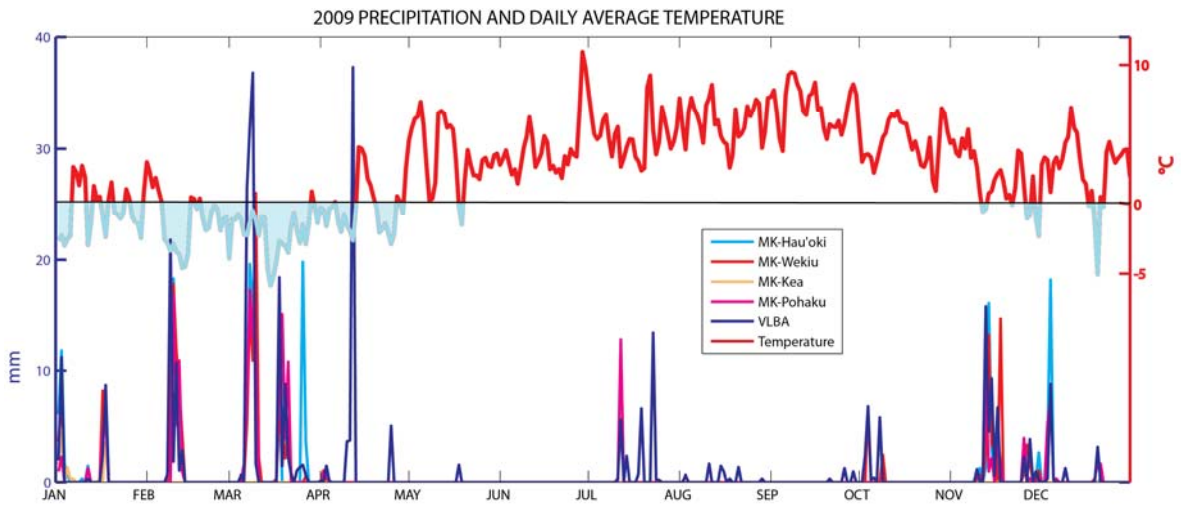
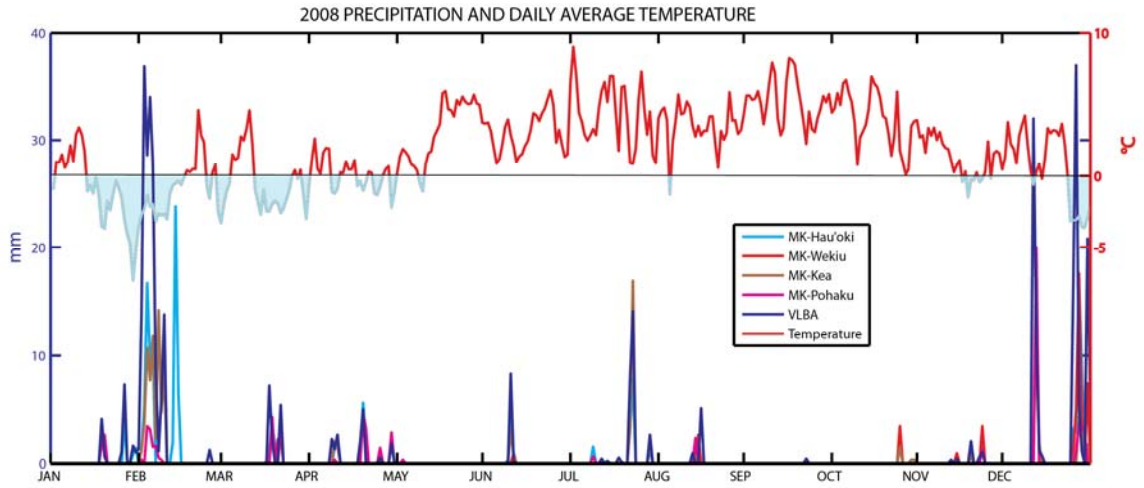


Fig. 3: Summit precipitation (mm) from listed weather stations and average daily temperature ( $^{\circ}$  C) over entire year, a) 2008; b) 2009; c) 2010.

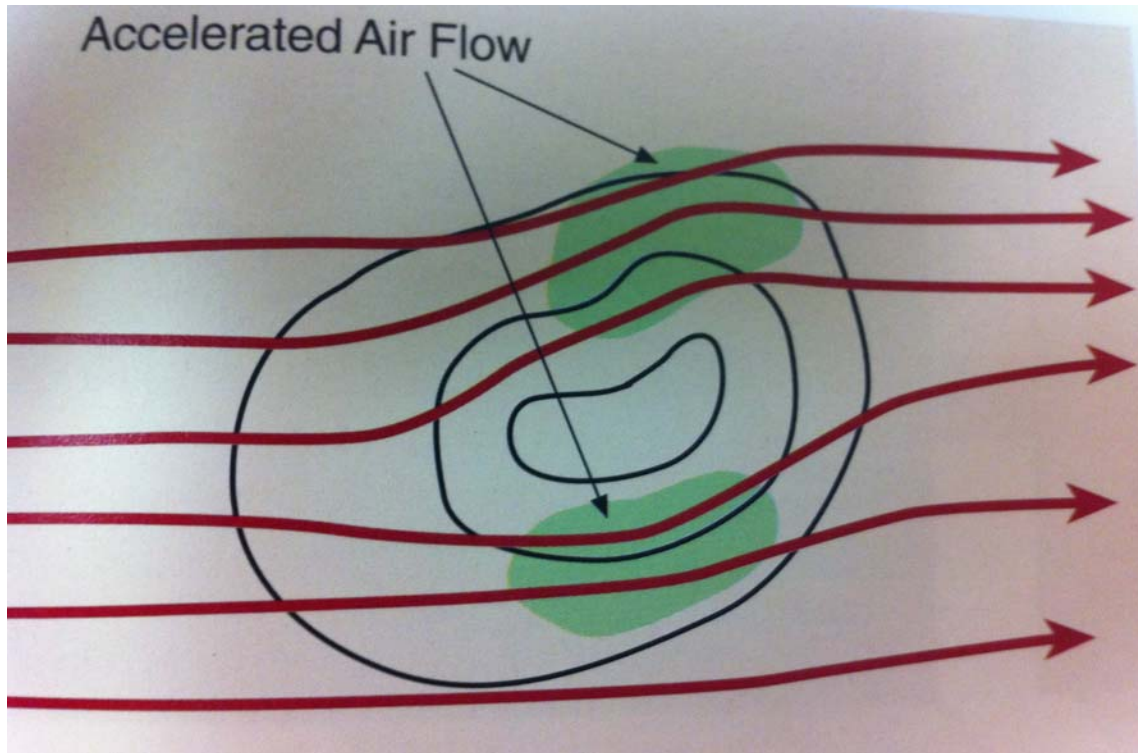


Fig. 4: Strong wind zones indicated by green shading are produced on the edges of the hill that are tangent to the flow (Whiteman, 2000).

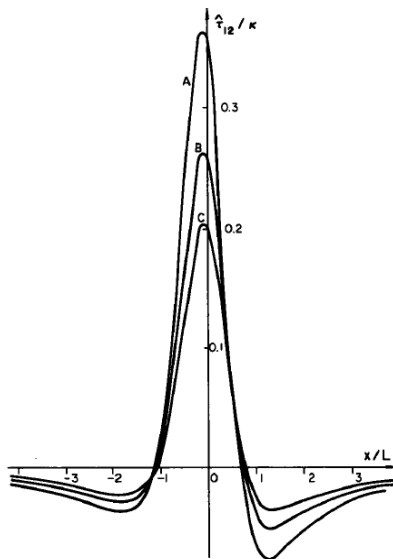
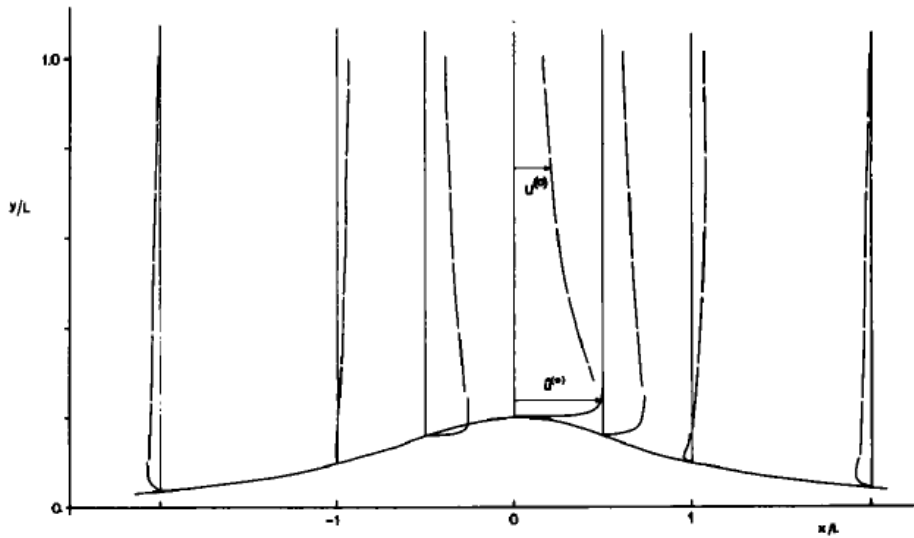
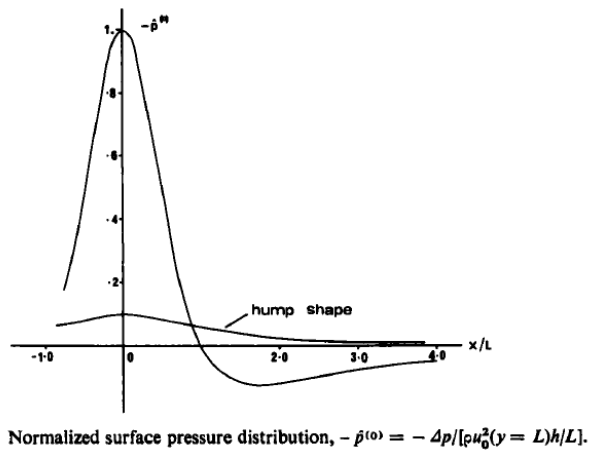


Fig. 5: a) Normalized surface pressure distribution; b) normalized perturbation velocity profiles at different positions over a hill; c) normalized surface shear stress perturbations with decreasing surface roughness.



Fig. 6: Wekiu bug feeding on dead bug fall. (Photo by: J. Eiben)

# MAUNA KEA SUMMIT

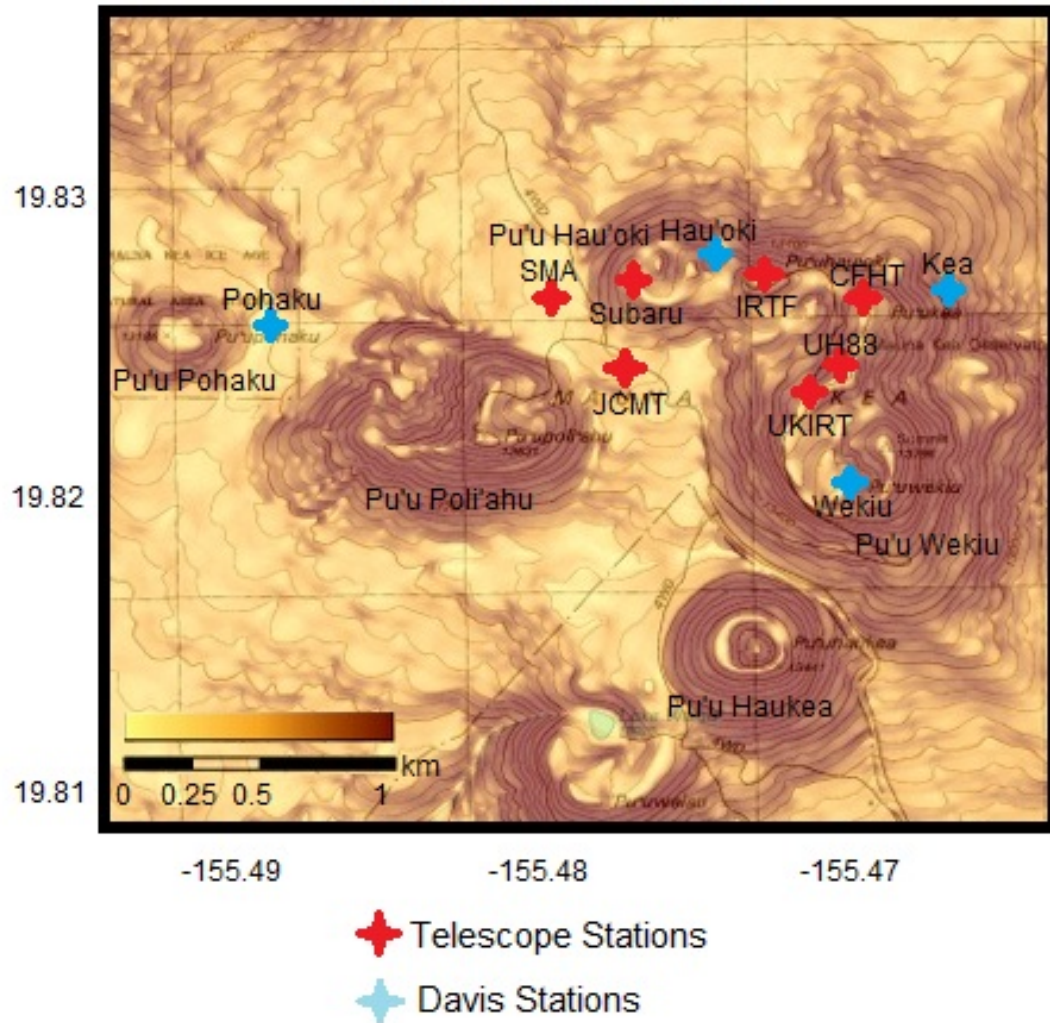


Fig. 7: Study area spans from 19.808 N to 19.837 N and -155.495 W to -155.455W, a 140400 m<sup>2</sup> area. Plotted are locations of Davis weather stations (blue) and telescope weather stations (red).

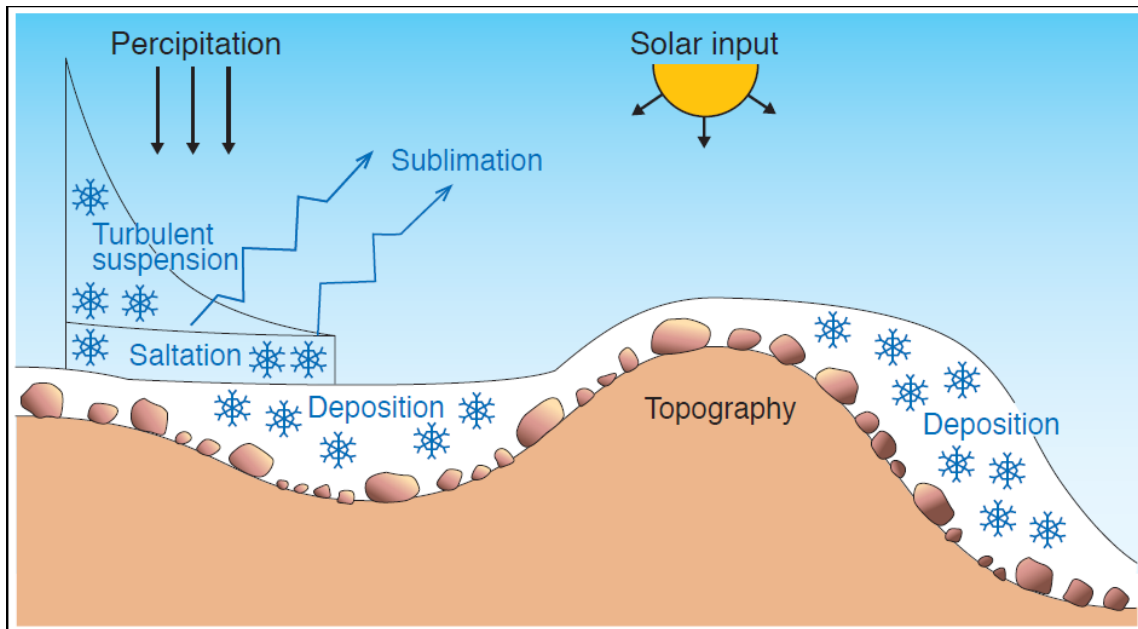


Fig. 8: Key features of the snow-transport model (after Liston et al., 2007)

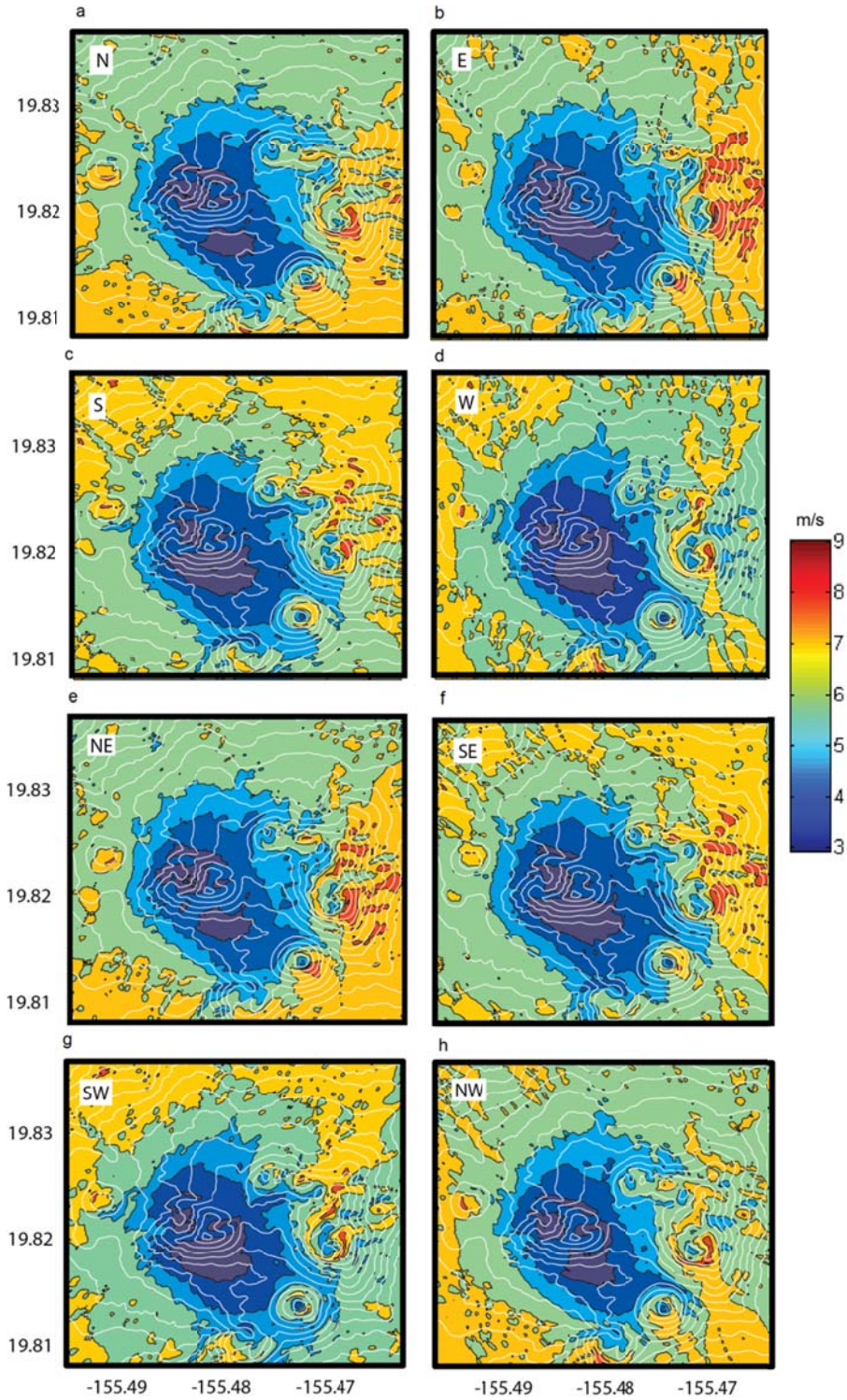


Fig. 9: Modeled wind speed from cardinal and intercardinal wind fields; a) north ; b) east; c) south; d) west; e) northeast; f); southeast; g)southwest; h) northwest.

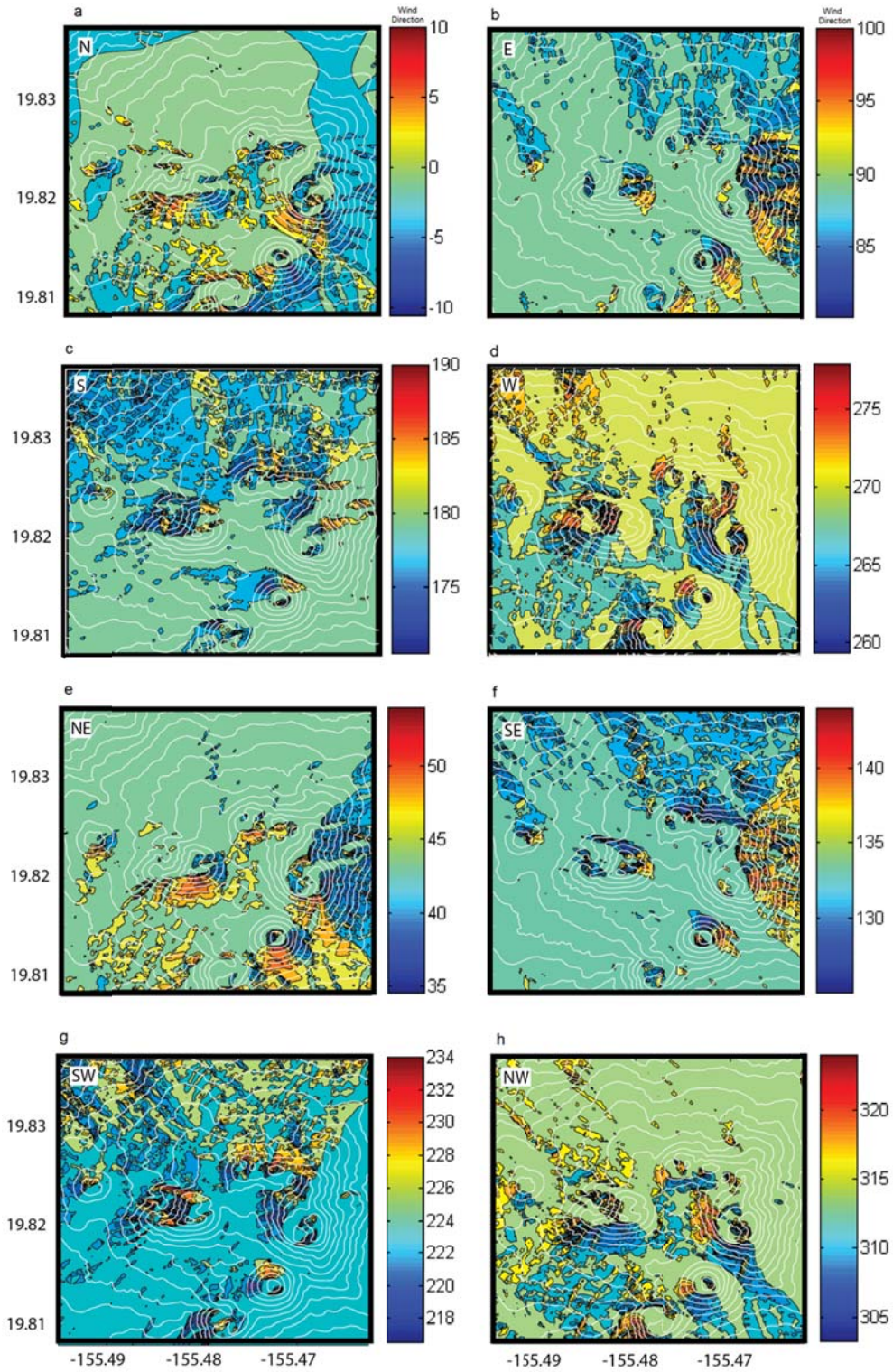


Fig. 10: Modeled wind direction from cardinal and intercardinal wind fields; a) north ; b) east; c) south; d) west; e) northeast; f); southeast; g)southwest; h) northwest.

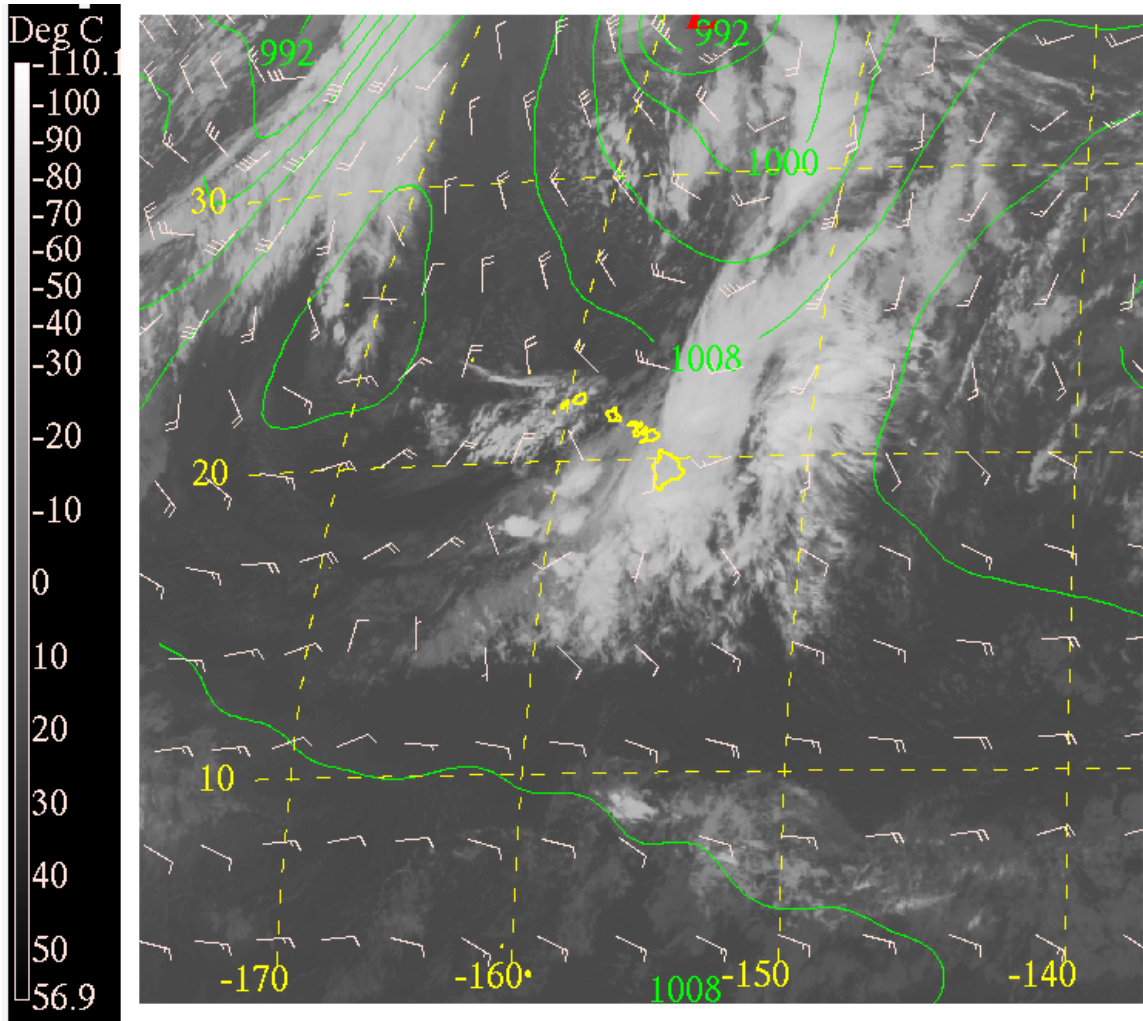


Fig. 11: VIS satellite image – 11 JANUARY 2011 at 0600 UTC, with initial analysis from GFS of sea level pressure (mb) and winds (krs)

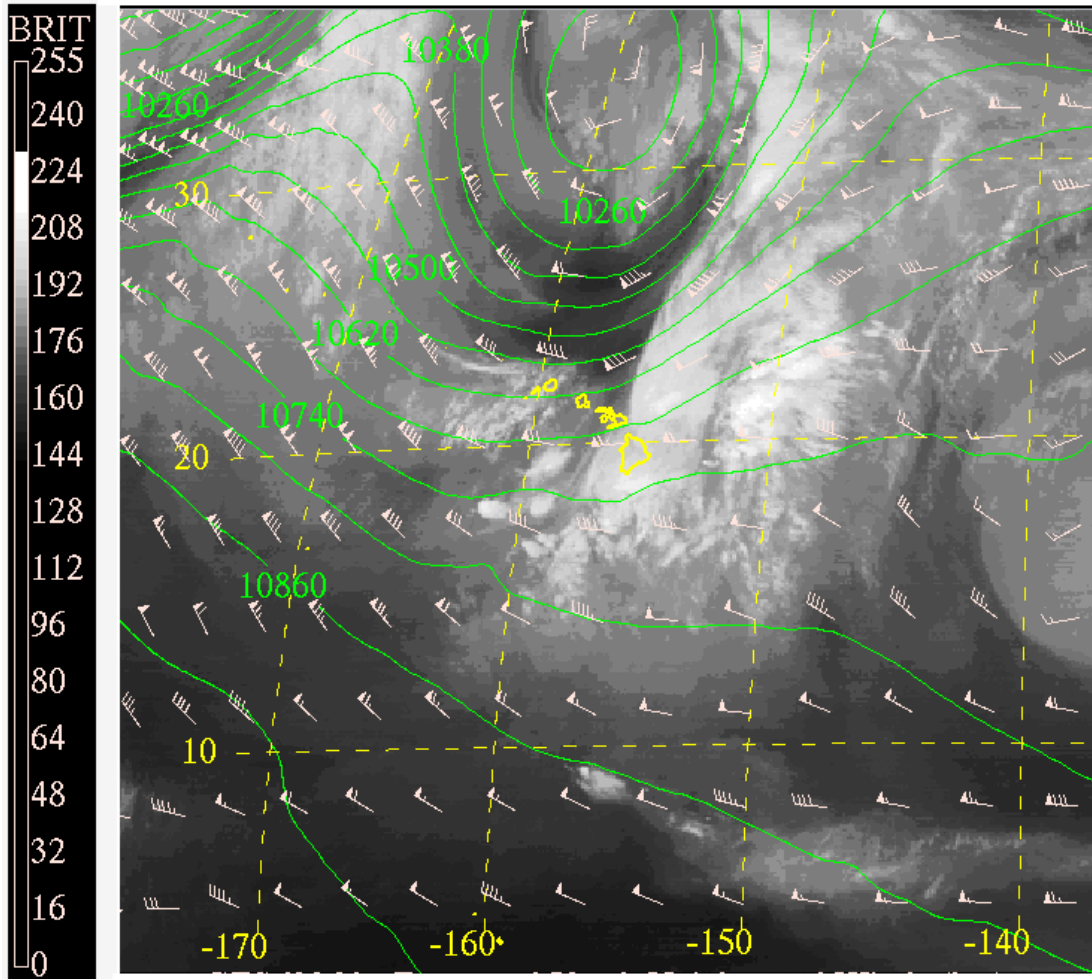


Fig. 12: WV satellite image – 11 JANUARY 2011 at 0600 UTC, with initial analysis from GFS model of 250mb Heights and Winds (kts)



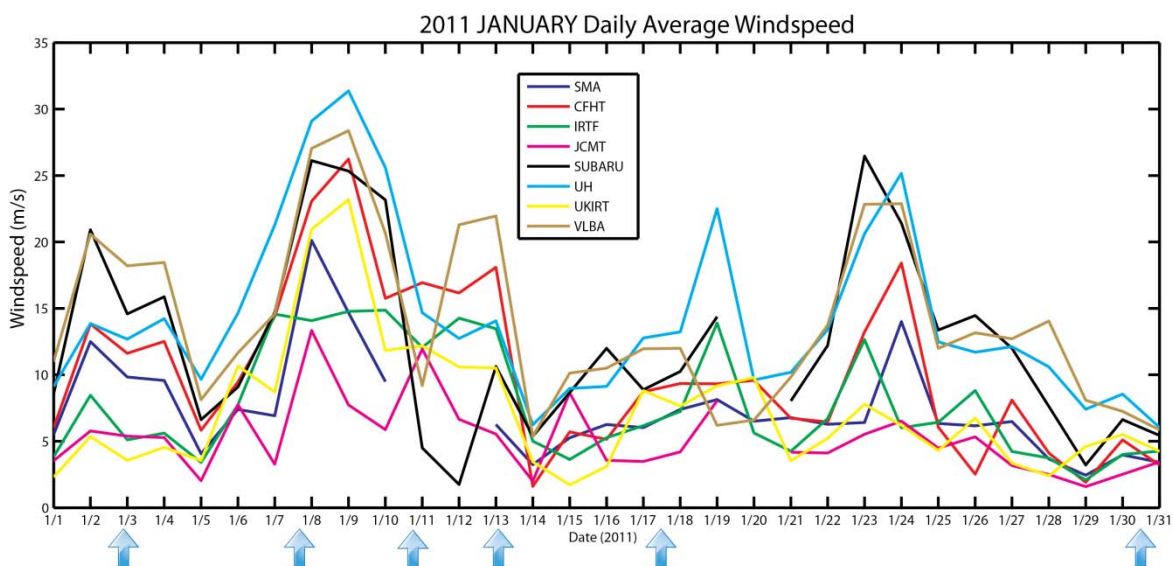
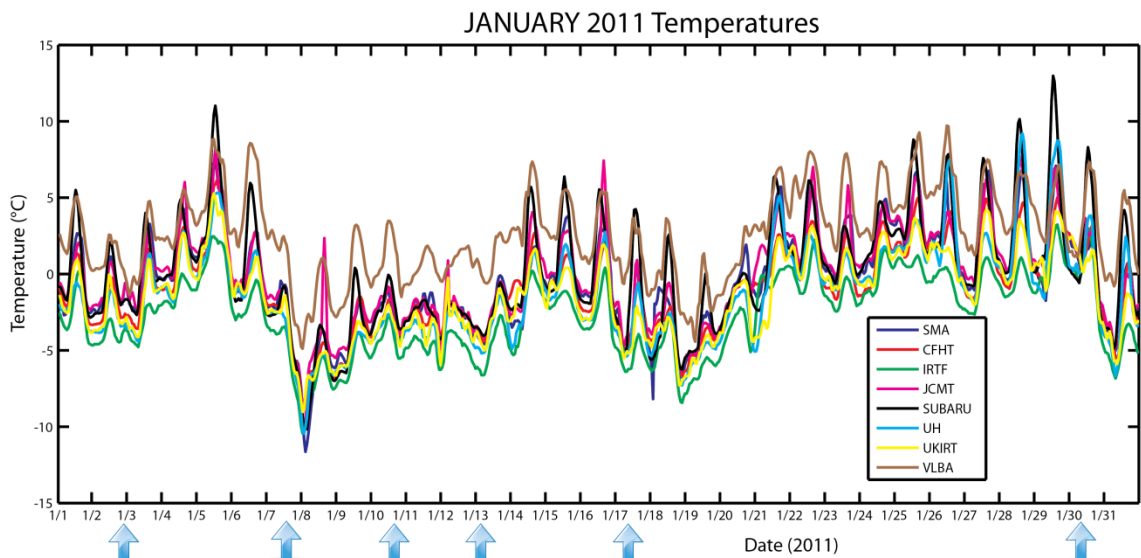


Fig. 14: Mauna Kea summit a) average hourly temperatures b) average daily wind speed for January 2011. Blue arrows indicate snow events during January 2011.

## 09-11 JANUARY 2011 Summit Winds

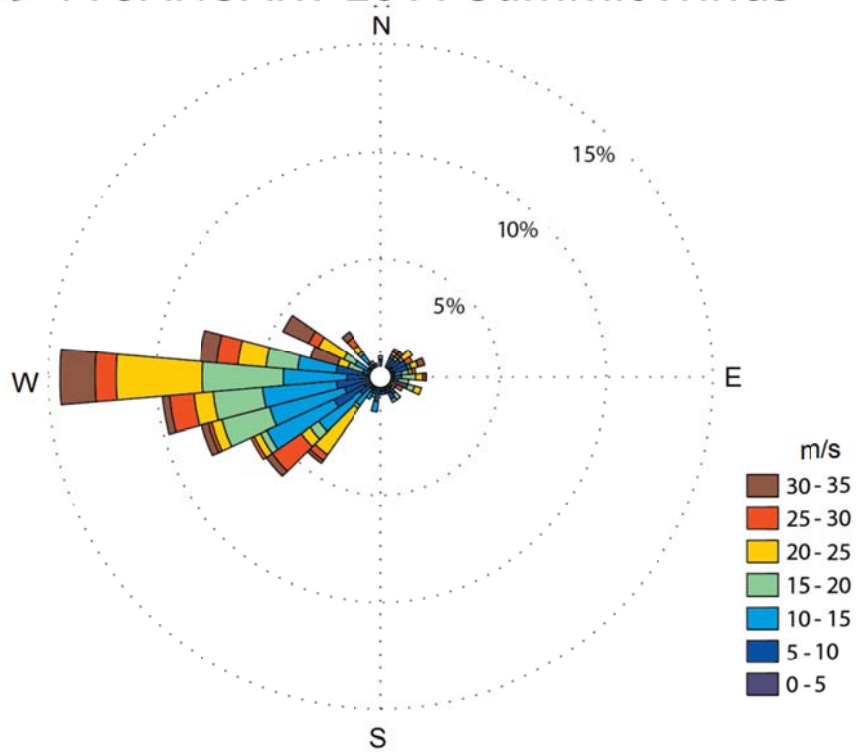


Fig. 15: Windrose plot of Mauna Kea summit wind speeds and directions from 1000 UTC 09 January to 0900 UTC 11 JANUARY 2011.



Fig. 16: Field experiment on 11 JANUARY 2011; a) Pu'u Hau'oki during field experiment, taking snowdepth measurements (Photo by C.R.S. Chambers); b) ruler showing depth in cm (Photo by L. Eaton).

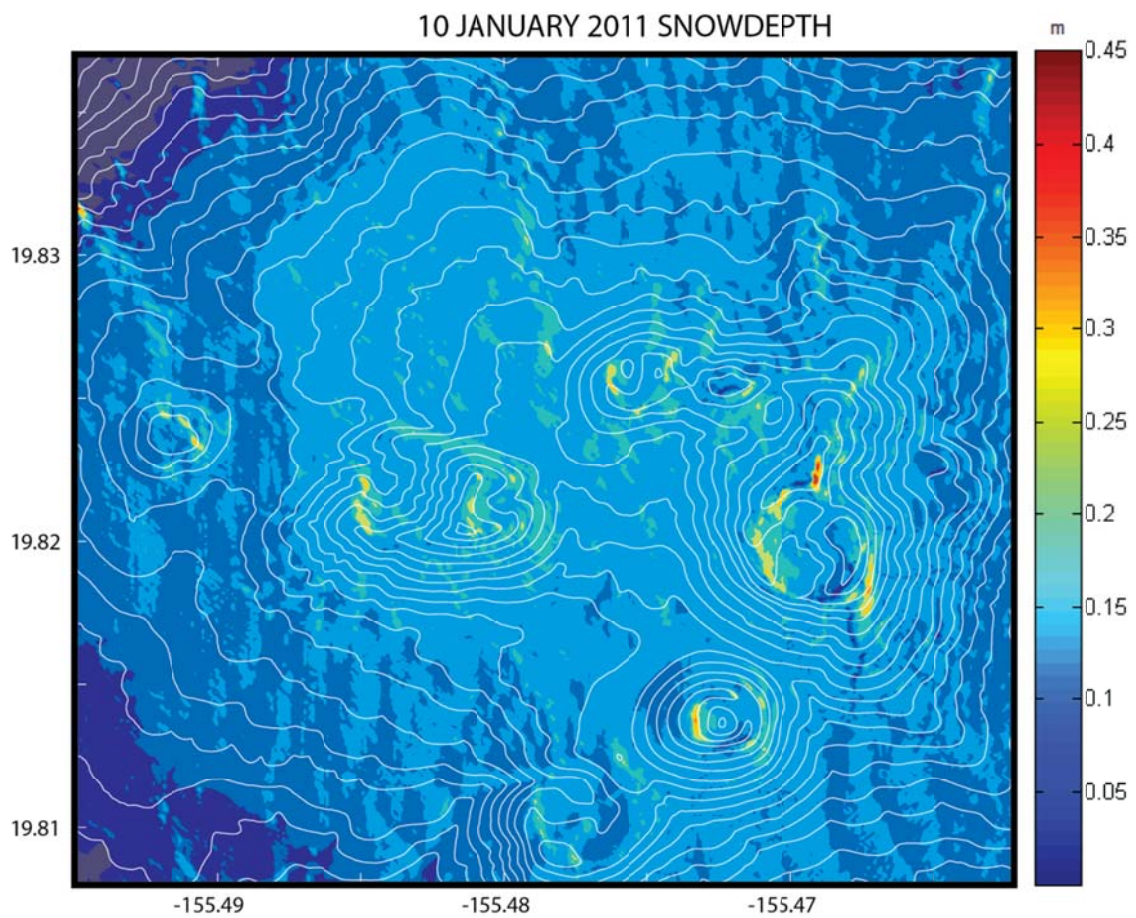


Fig. 17: SnowModel output, snowpeth in meters (colored), height contours (black) for 0959 UTC 11 JANUARY 2011.

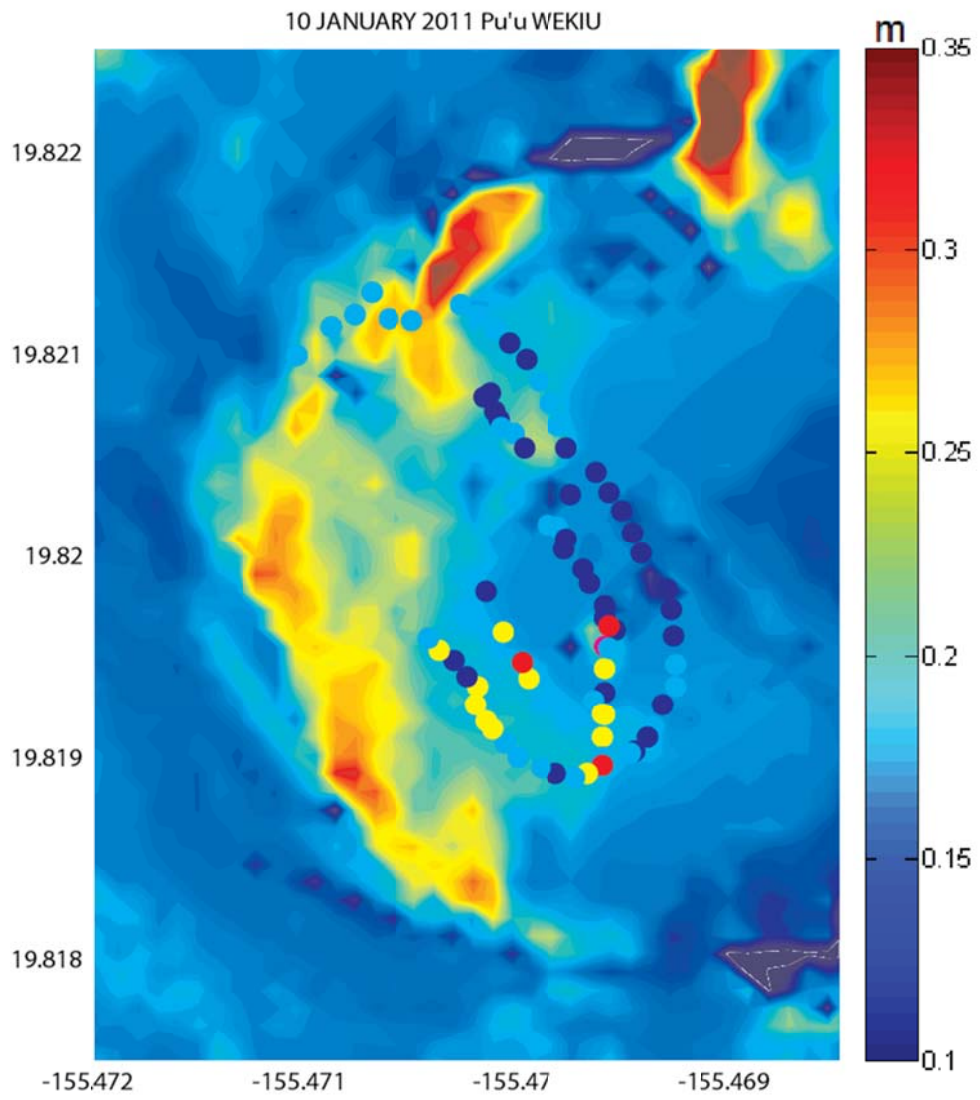


Fig. 18: Pu'u Wēkiu modeled snowpeth (color contours) for 0959 UTC 11 January 2011, snowdepth observations (colored dots) between 2130 UTC 11 January and 0000 UTC 12 January 2011.

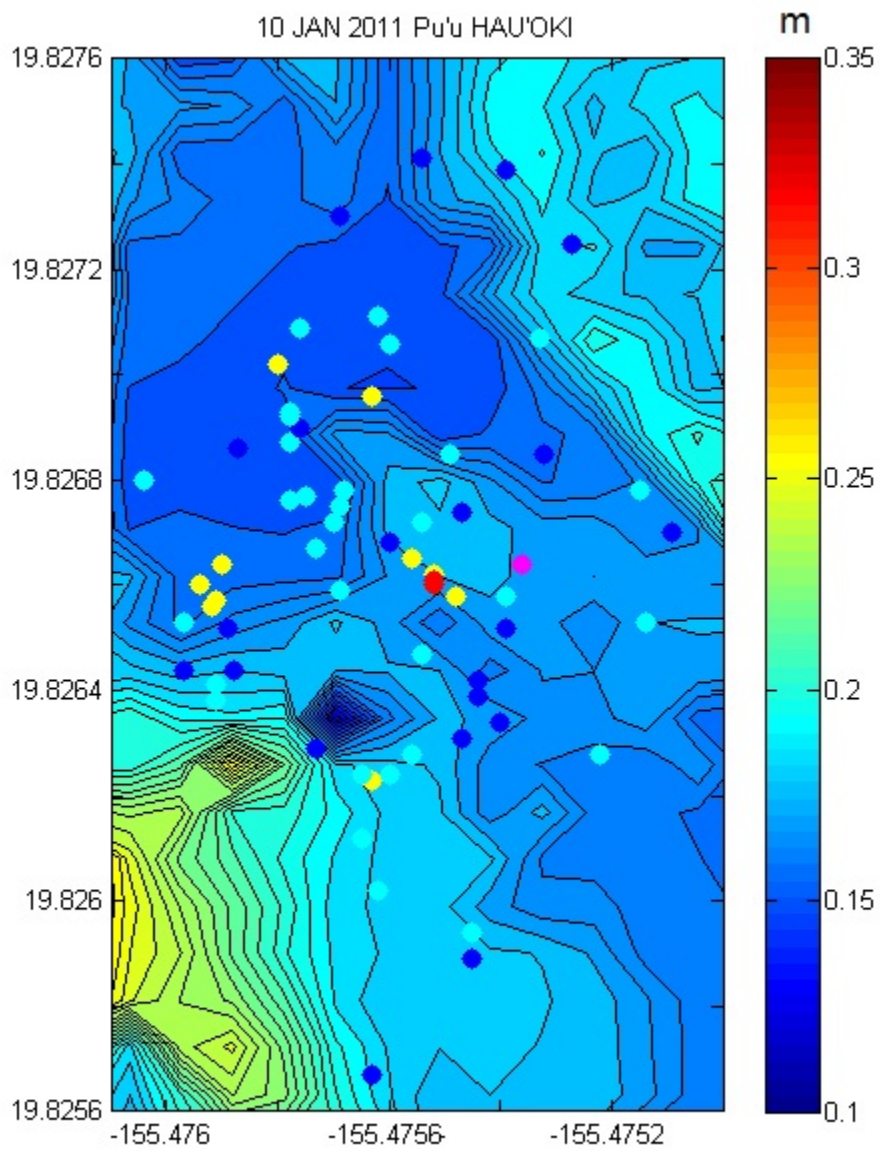


Fig. 19: Same as Fig. 18, but for Pu'u Hau'oki.

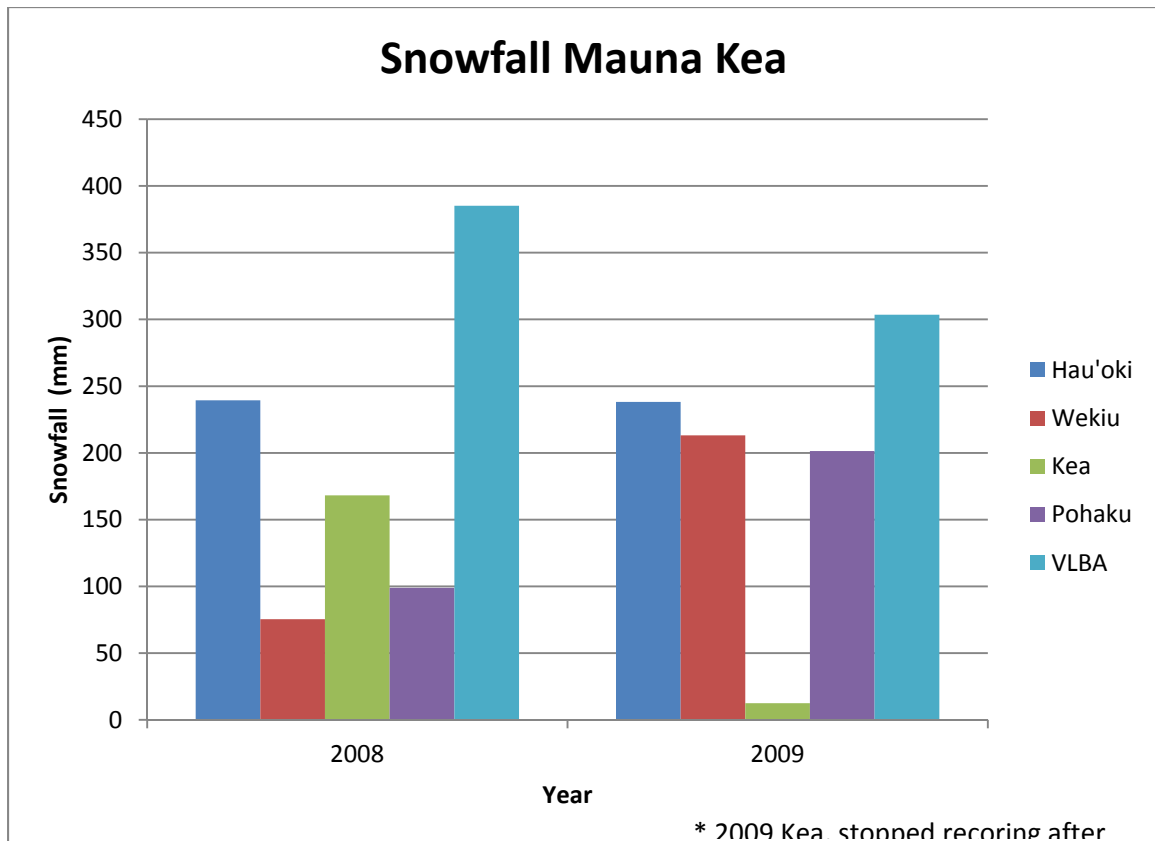


Fig. 20: Mauna Kea yearly snowfall accumulation (mm) for 2008, 2009).

# 2008 MAUNA KEA SUMMIT WINDS

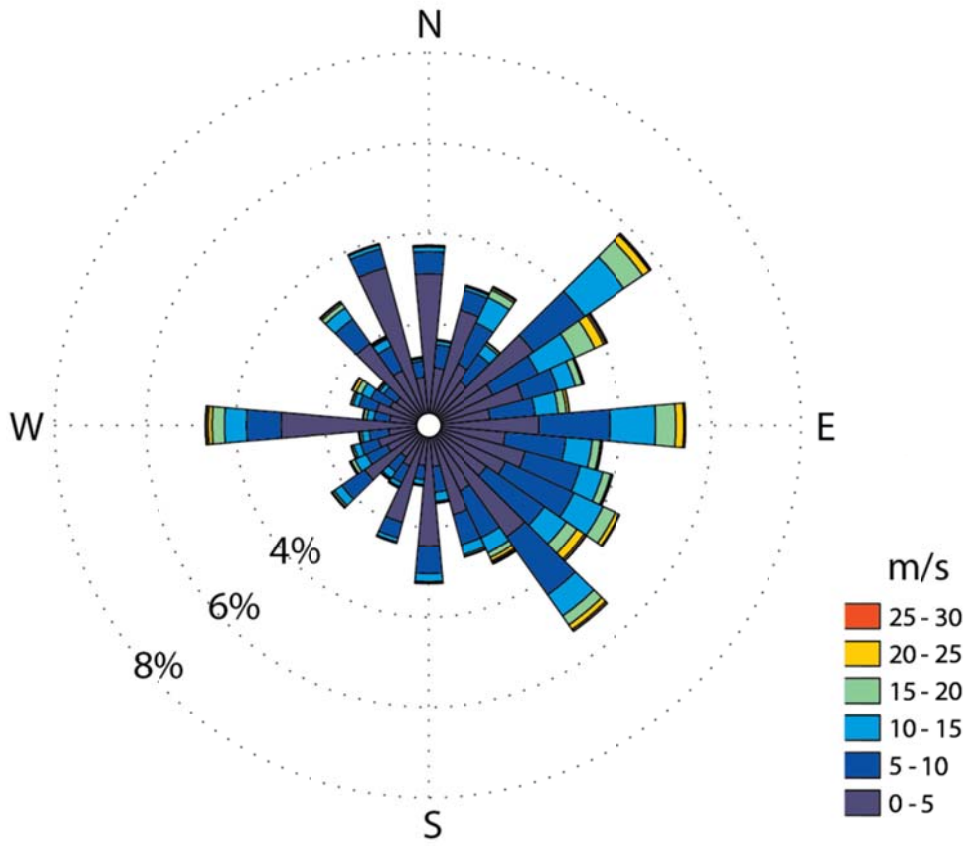
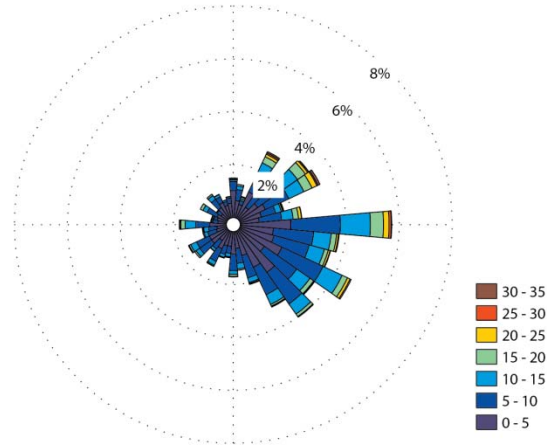
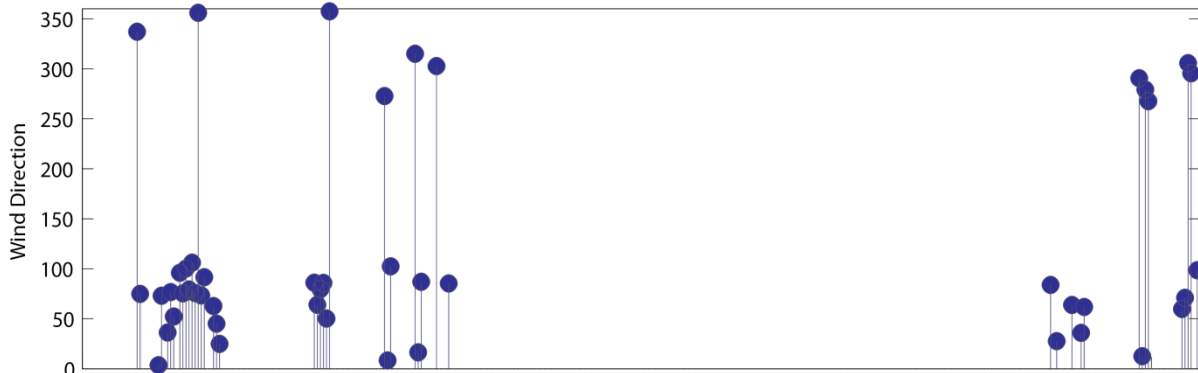


Fig. 21: Windrose for all 2008 Mauna Kea summit winds

### 2008 WINDS DURING SNOW EVENTS



### 2008 SNOW EVENT WIND DIRECTION



### 2008 SNOW EVENT PRECIPITATION AND DAILY AVERAGE TEMPERATURE

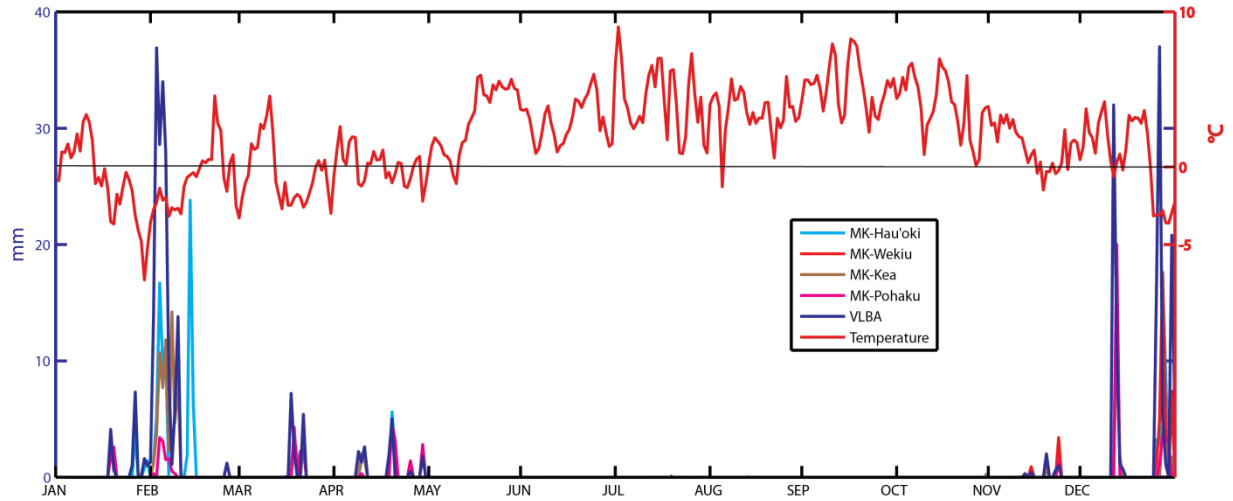


Fig 22: a) Windrose of winds during snow events for 2008 , b) snow event average wind direction, temperature, and daily precipitation.

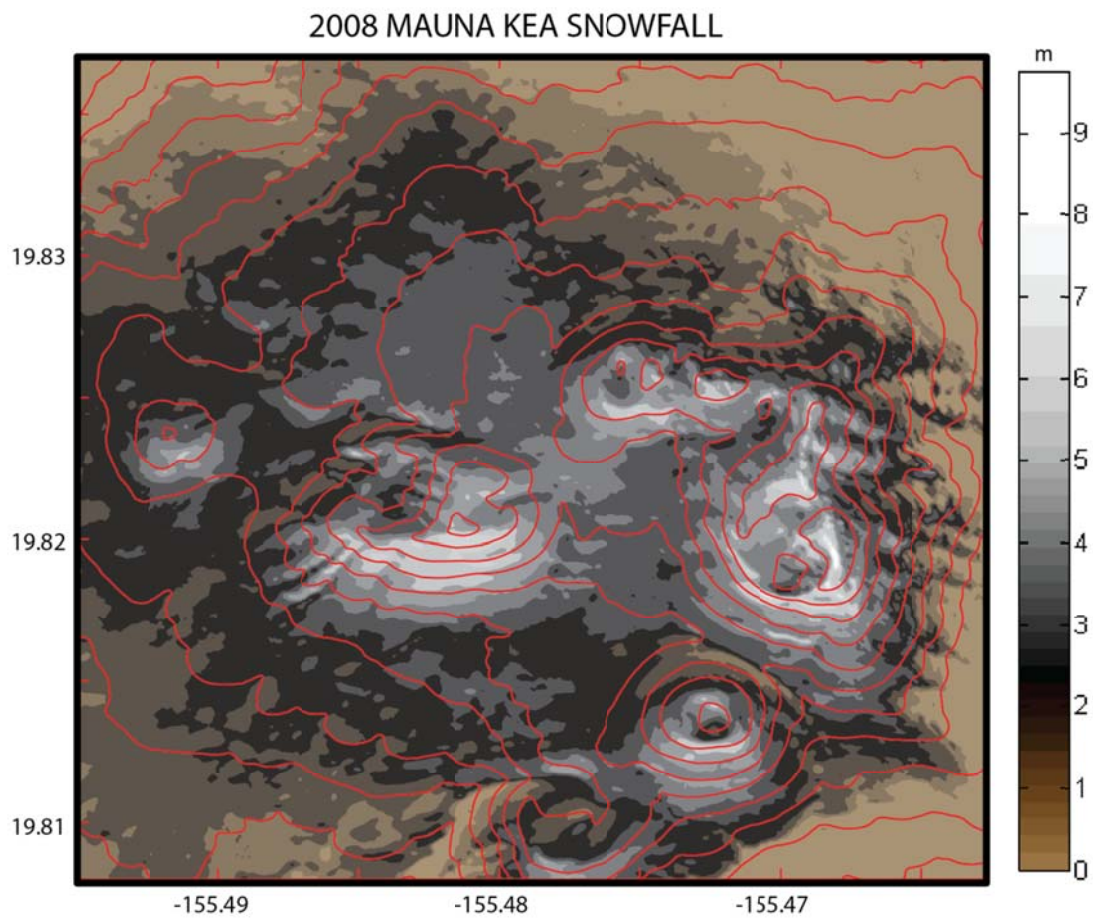


Fig. 23: Modeled snowdepth in meters (color contours) and elevation (red contours) of Manna Kea summit for 2008.

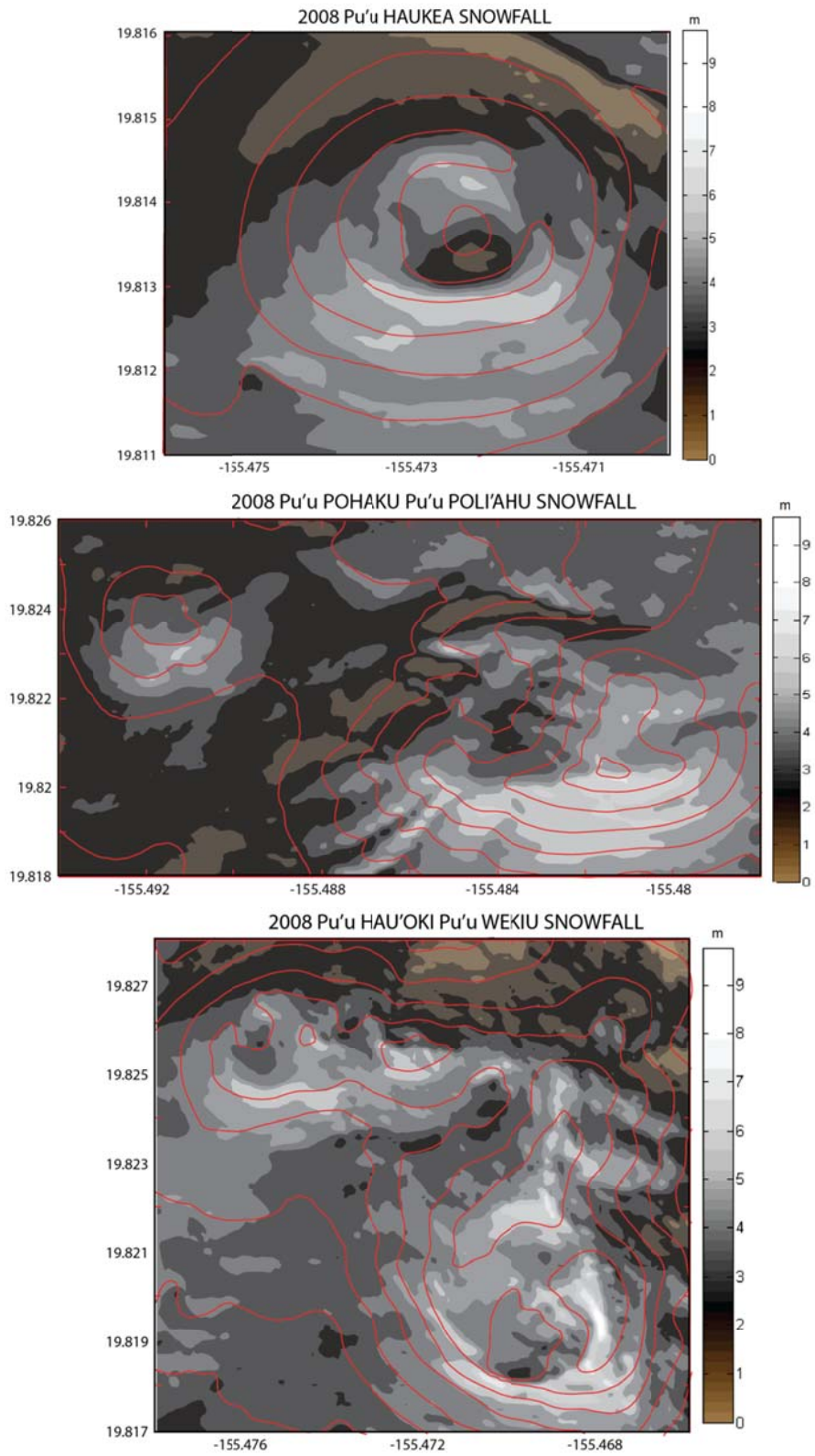


Fig 24: Same as Fig. 23 but for a) Pu'u Haukea; b) Pu'u Pōhaku and Pu'u Poli'ahu; and c) Pu'u Hau'oki and Pu'u Wēkiu.

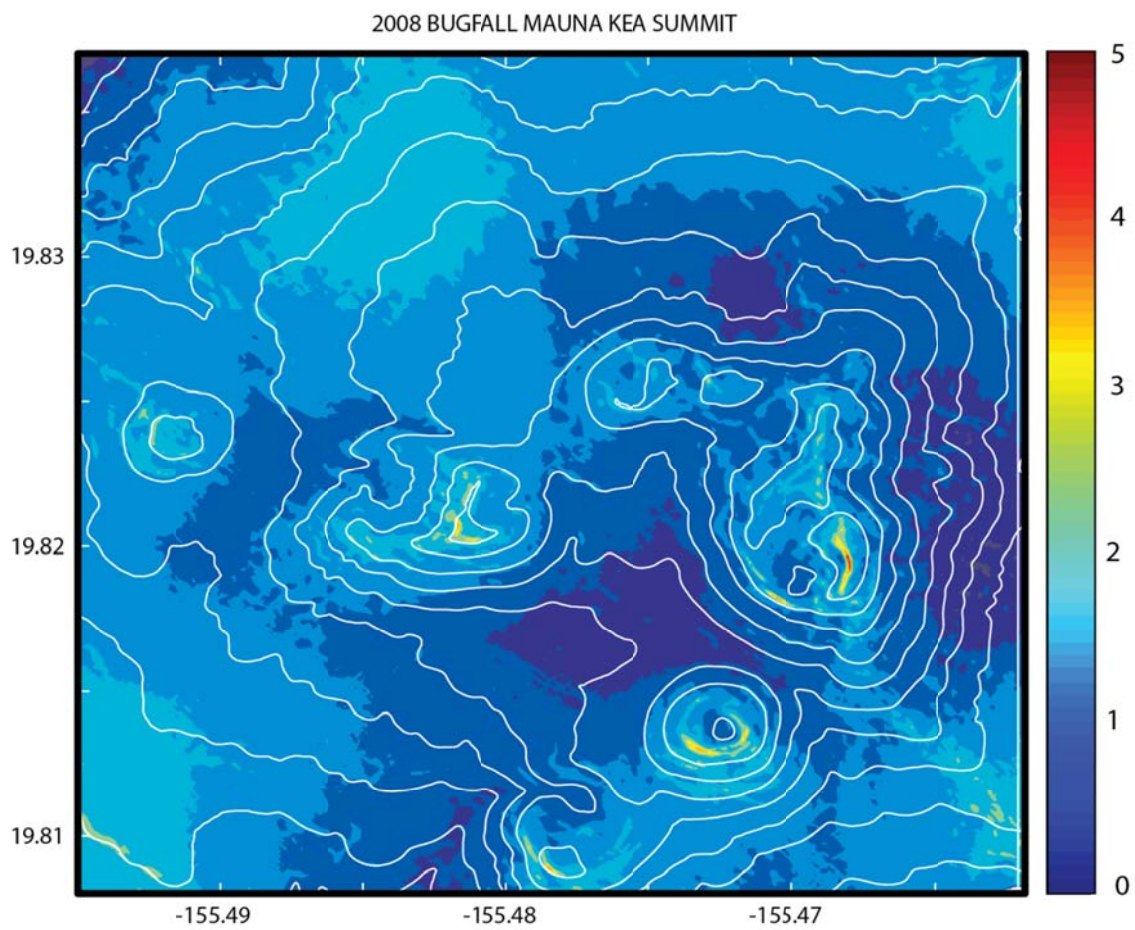


Fig. 25: Modeled bug fall accumulation (color contours) with elevation (white contours) on Mauna Kea summit for 2008.

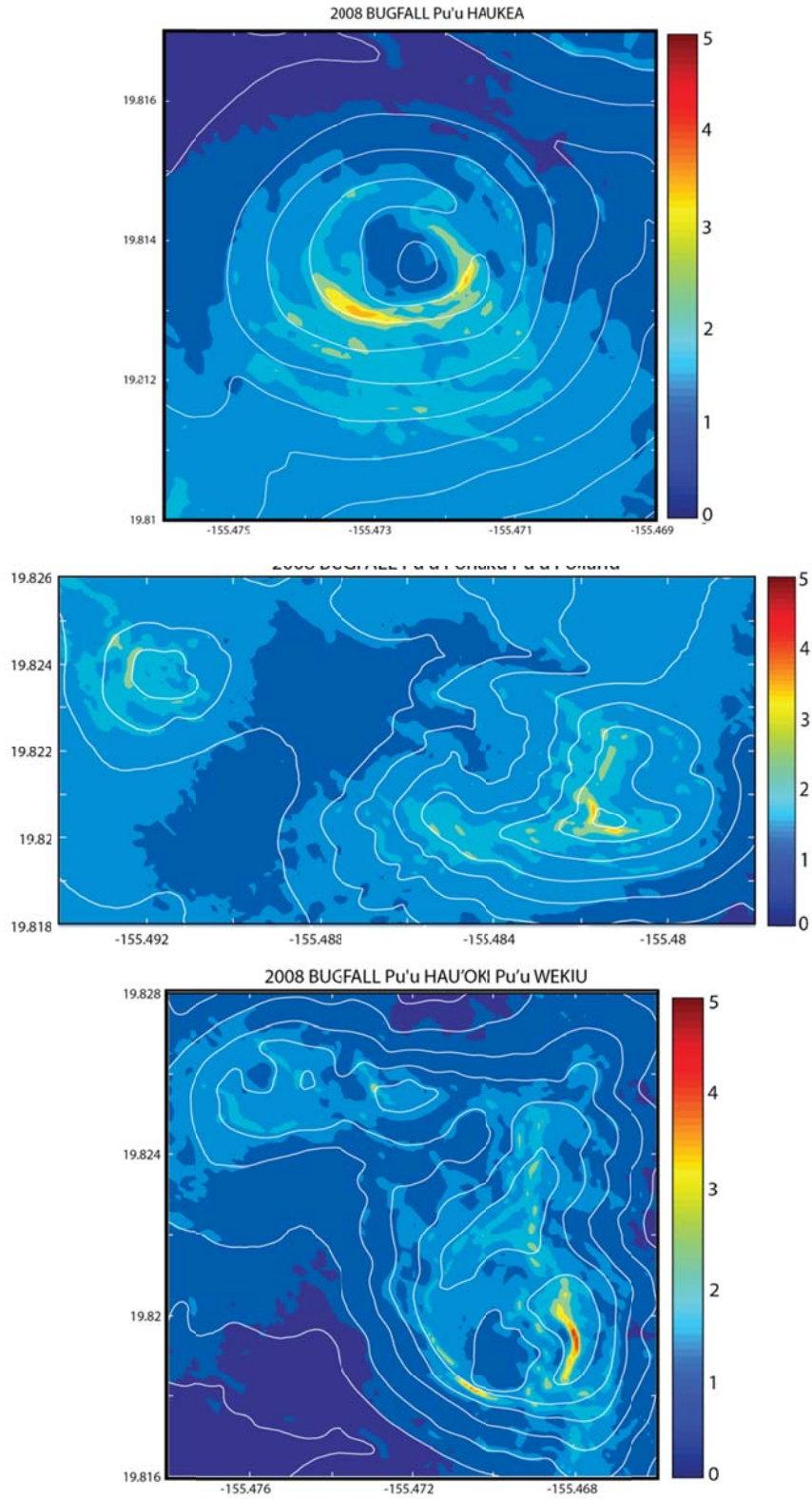


Fig. 26: Same as Fig. 25 but for a) Pu'u Haukea; b) Pu'u Pōhaku and Pu'u Poli'ahu; c) Pu'u Hau'oki and Pu'u Wēkiu.

# 2009 SUMMIT WINDS MAUNA KEA

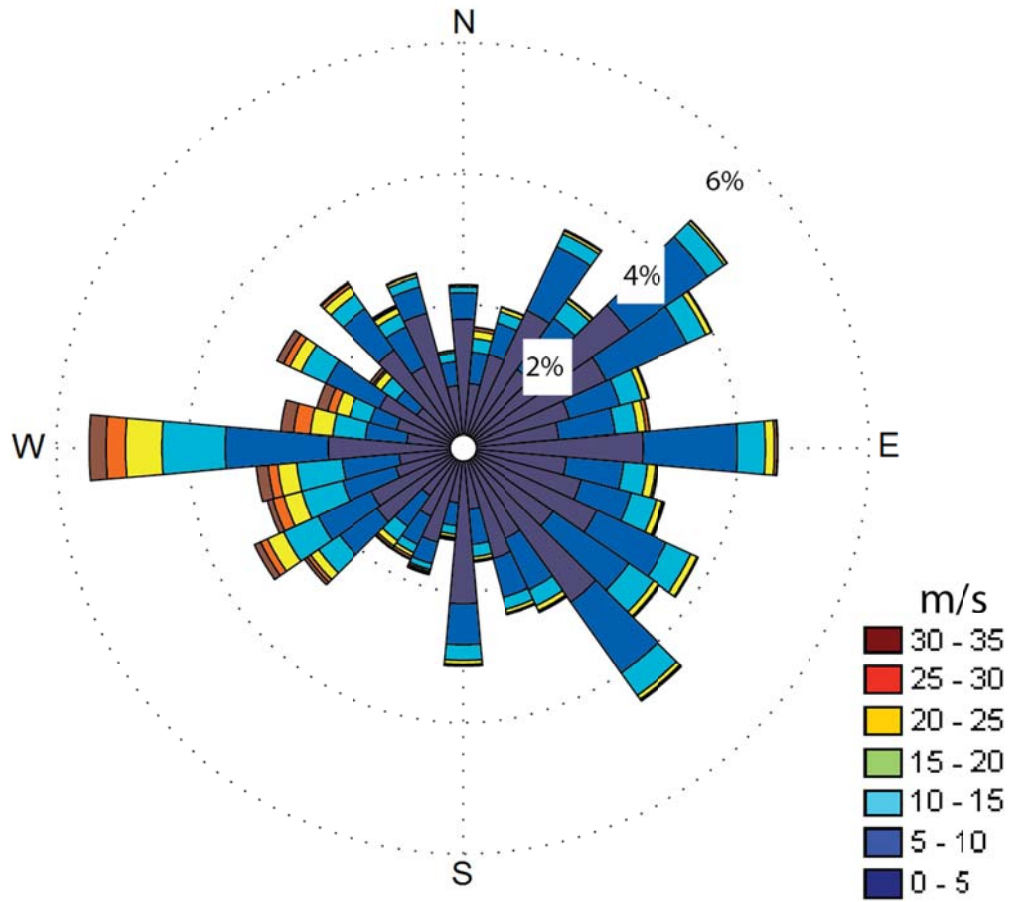


Fig. 27: Windrose for all 2009 Mauna Kea summit winds.

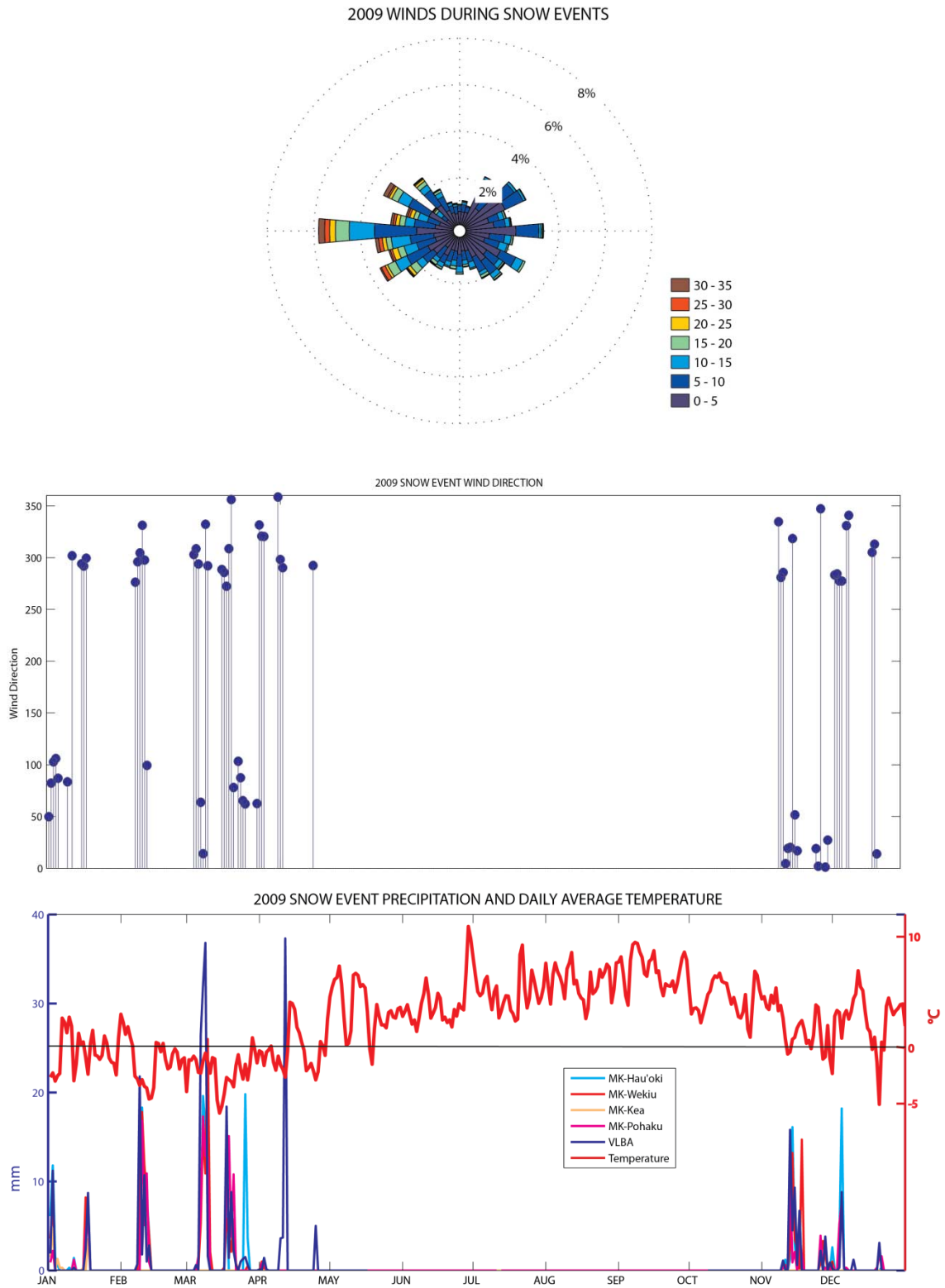


Fig. 28: a) Windrose of winds during snow events for 2009, b) snow event average wind direction, temperature, and daily precipitation.

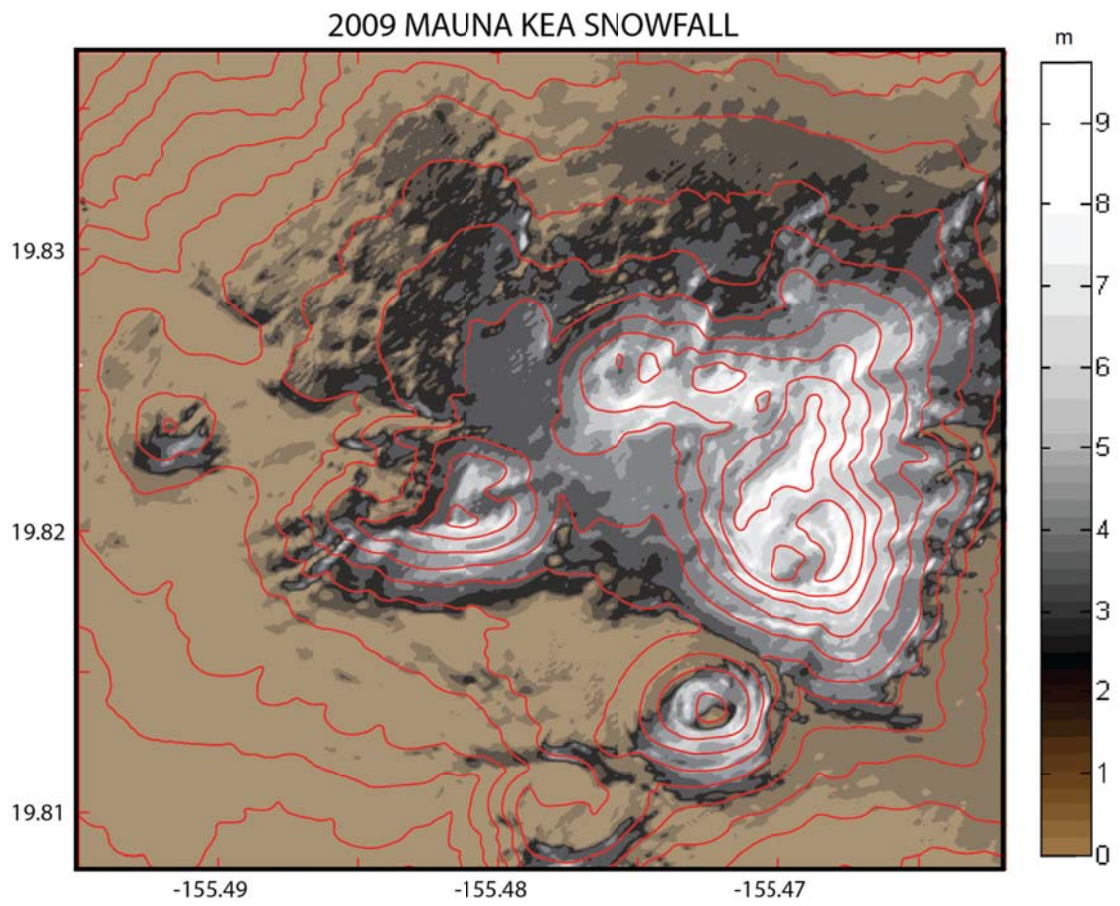


Fig. 29: Modeled snowdepth in meters (color contours) and elevation (red contours) of Muana Kea summit for 2009

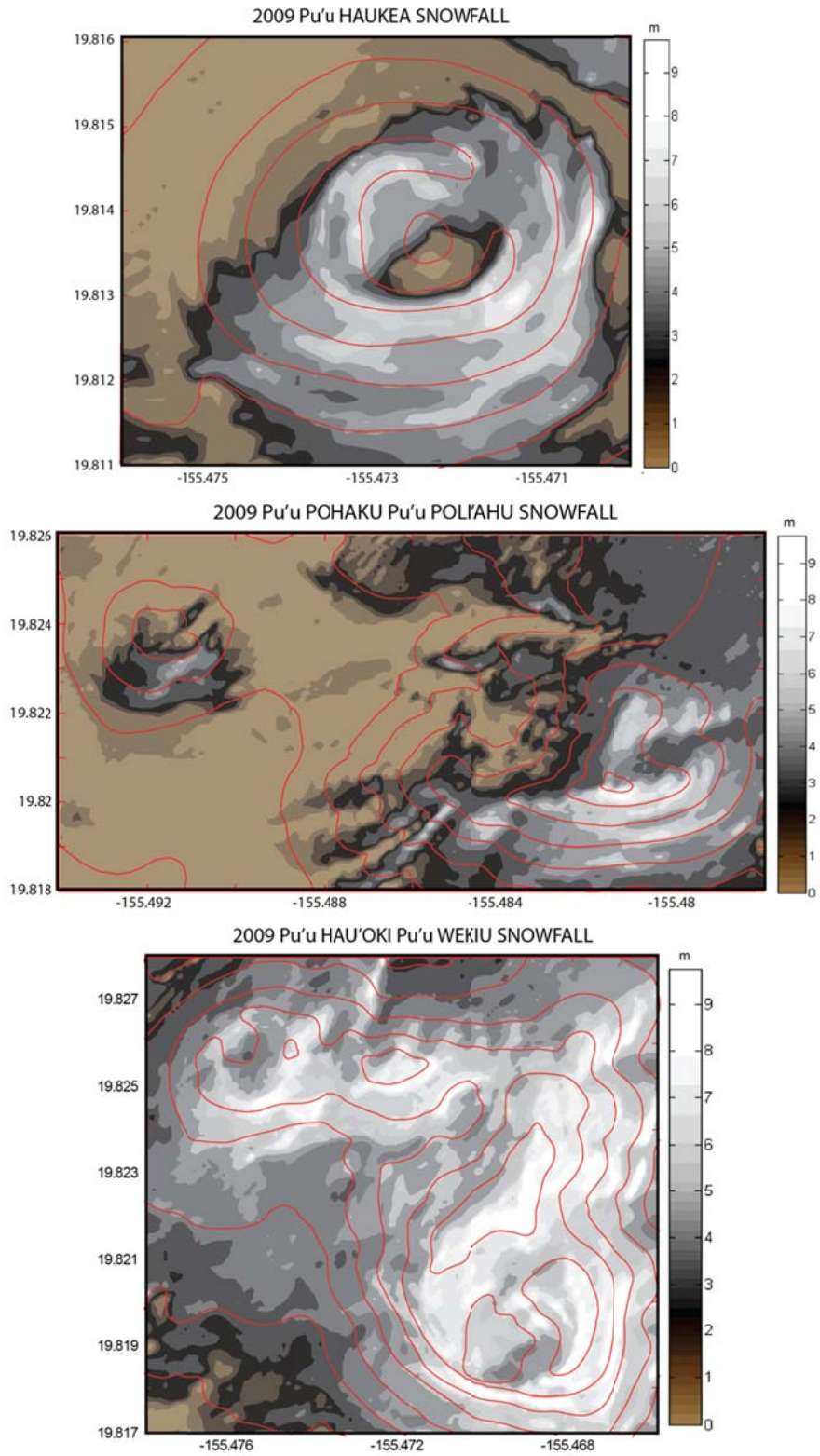


Fig 30: Same as Fig. 29 but for a) Pu'u Haukea; b) Pu'u Pōhaku and Pu'u Poli'ahu; and c) Pu'u Hau'oki and Pu'u Wēkiu

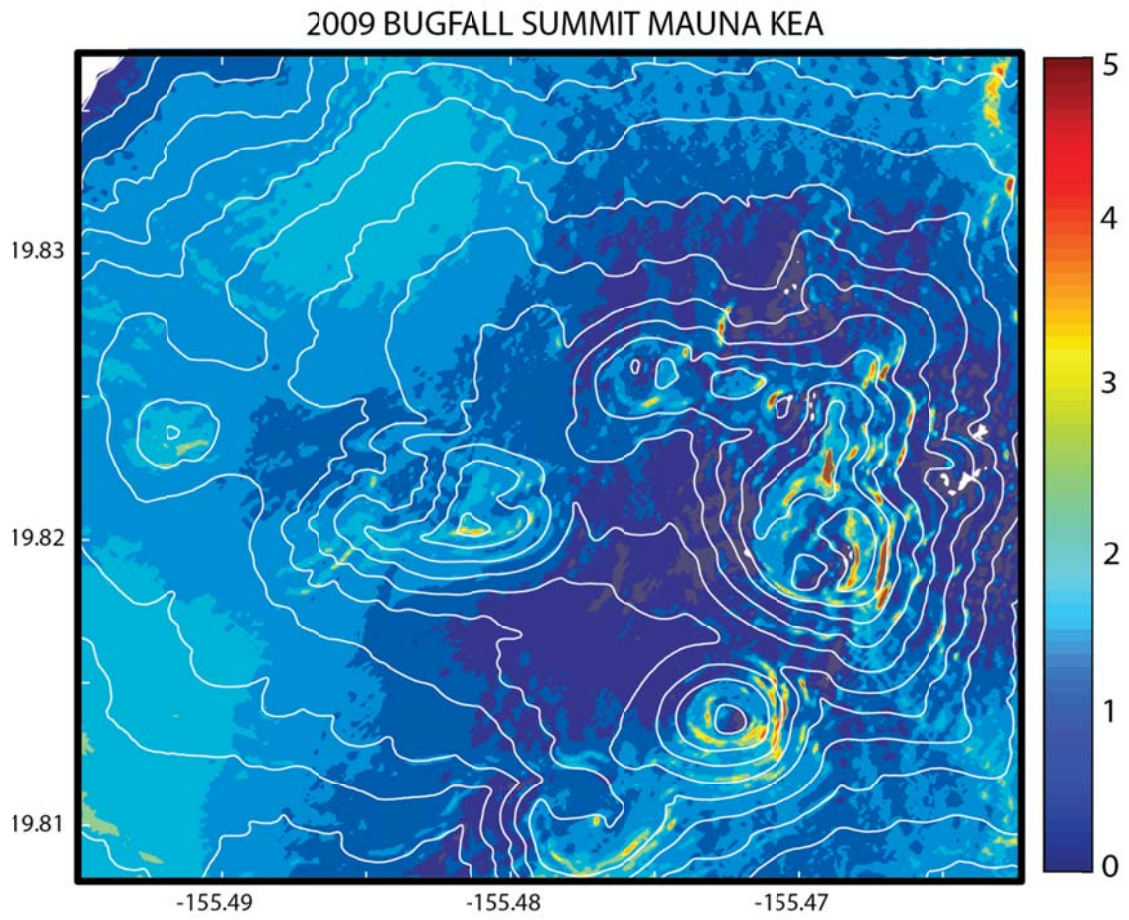


Fig. 31: Modeled bug fall density (color contours) with elevation (white contours) on Mauna Kea for 2009.

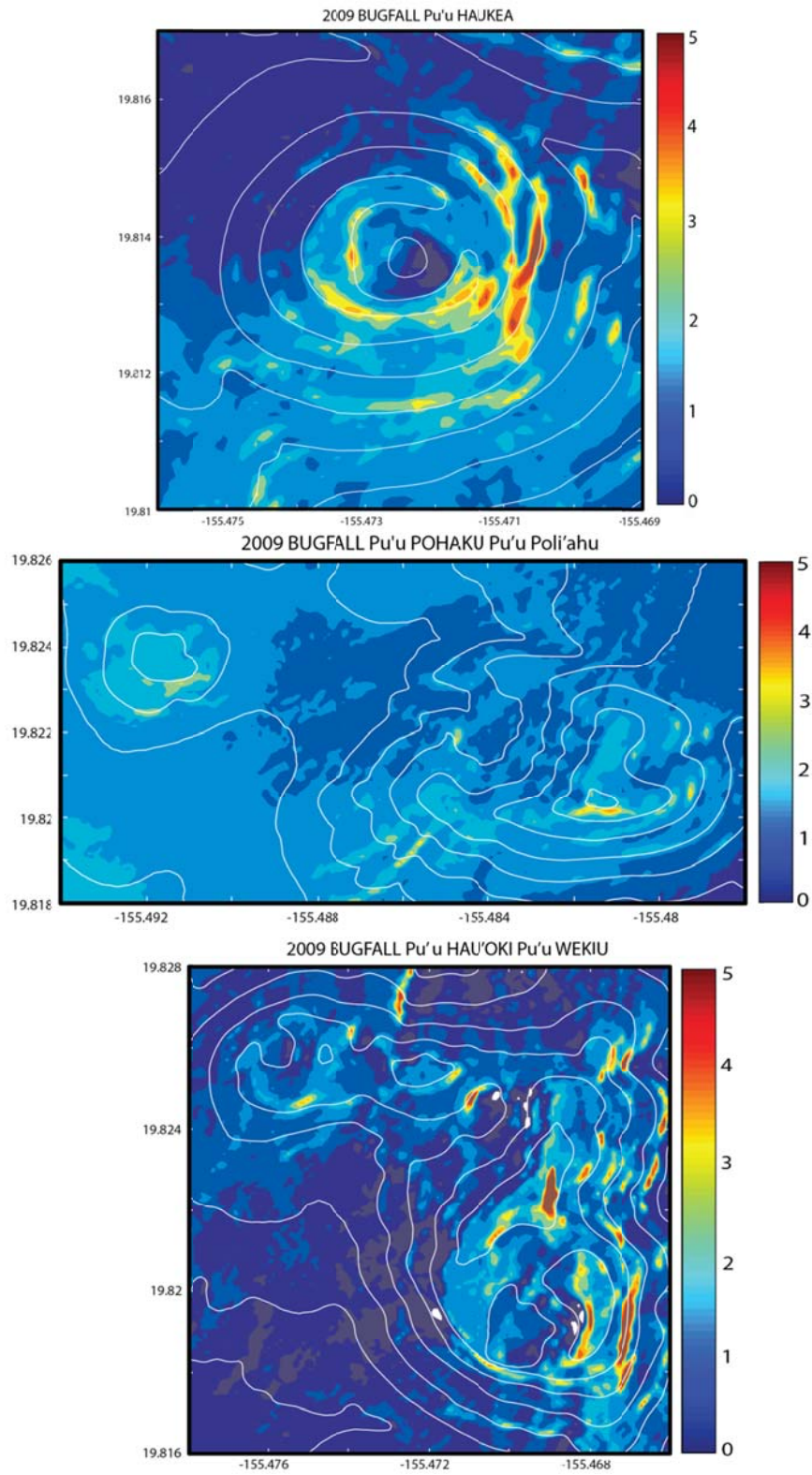


Fig. 32: Same as Fig. 31 but for a) Pu'u Haukea; b) Pu'u Pōhaku and Pu'u Poli'ahu; c) Pu'u Hau'oki and Pu'u Wēkiu

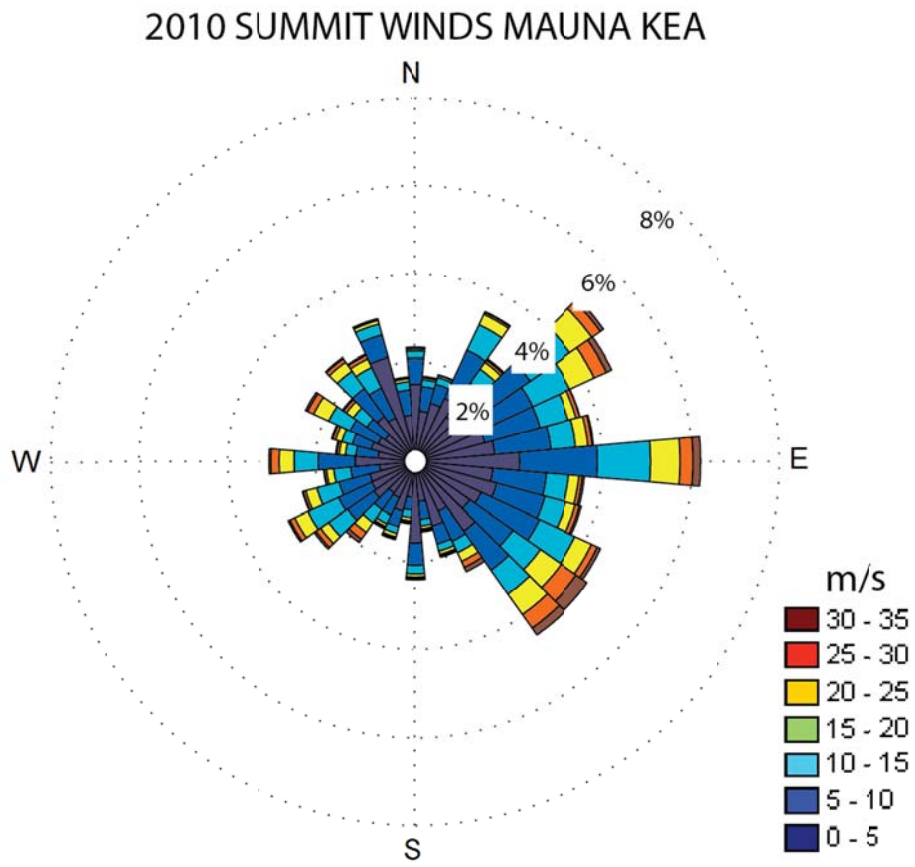


Fig. 33: Windrose for all 2010 Mauna Kea summit winds

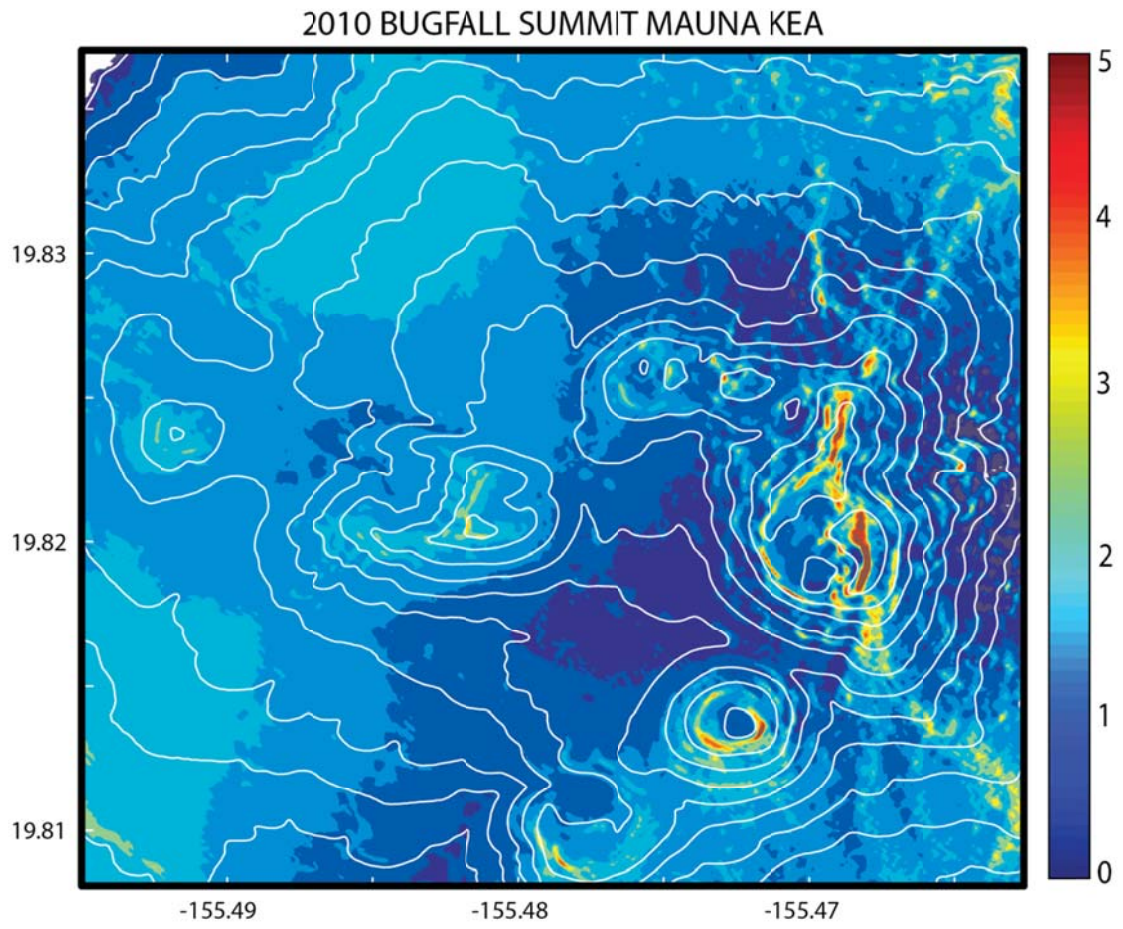


Fig. 34: Modeled bug fall density (color contours) with elevation (white contours) on Mauna Kea for 2010.

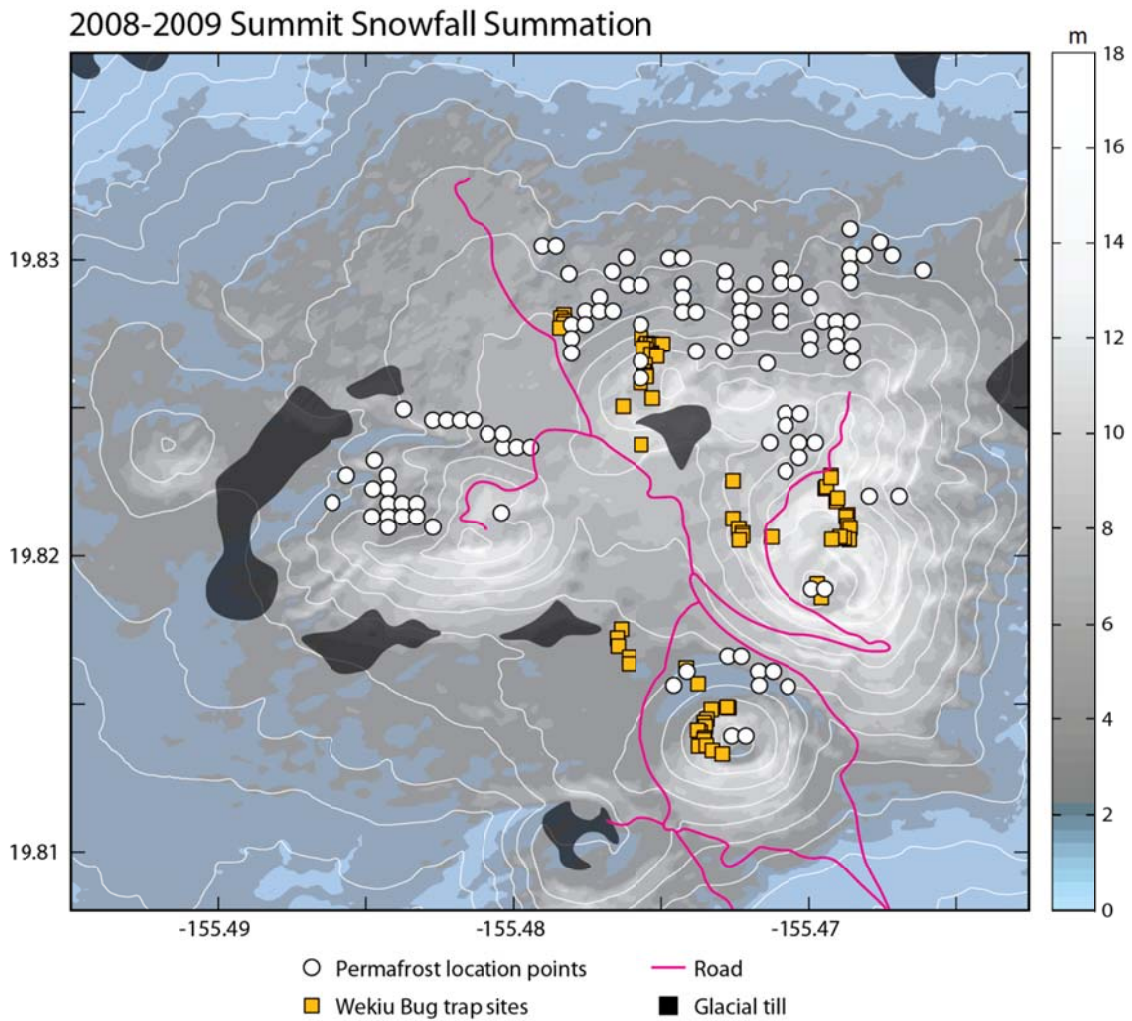


Fig. 35: Modeled snowdepth in meters (color contours) and elevation (red contours) of Muana Kea summit for the 2-year total from 2008-2009, and Wēkiu Bug trap locations from 2002-2008 with positive capture rates (yellow boxes), permafrost locations (white bubbles).

2008-2010 Bug fall Summit Mauna Kea and Wekiu Bug Traps

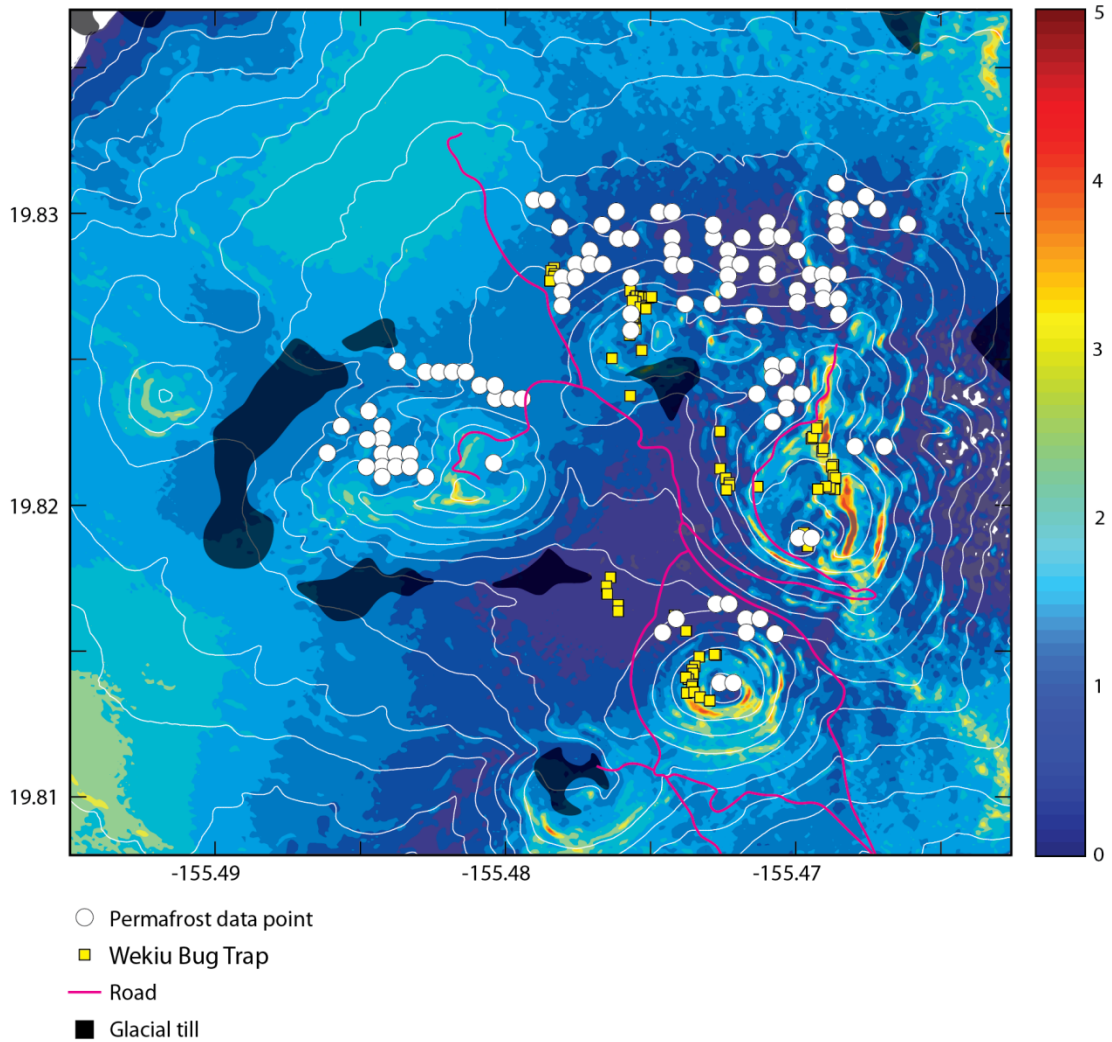


Fig. 36: Modeled bug fall density (color contours) with elevation (white contours) on Mauna Kea for 3-year total from 2008, 2009, 2010, and Wēkiu Bug trap locations from 2002-2008 with positive capture rate (yellow boxes), permafrost locations (white bubbles).

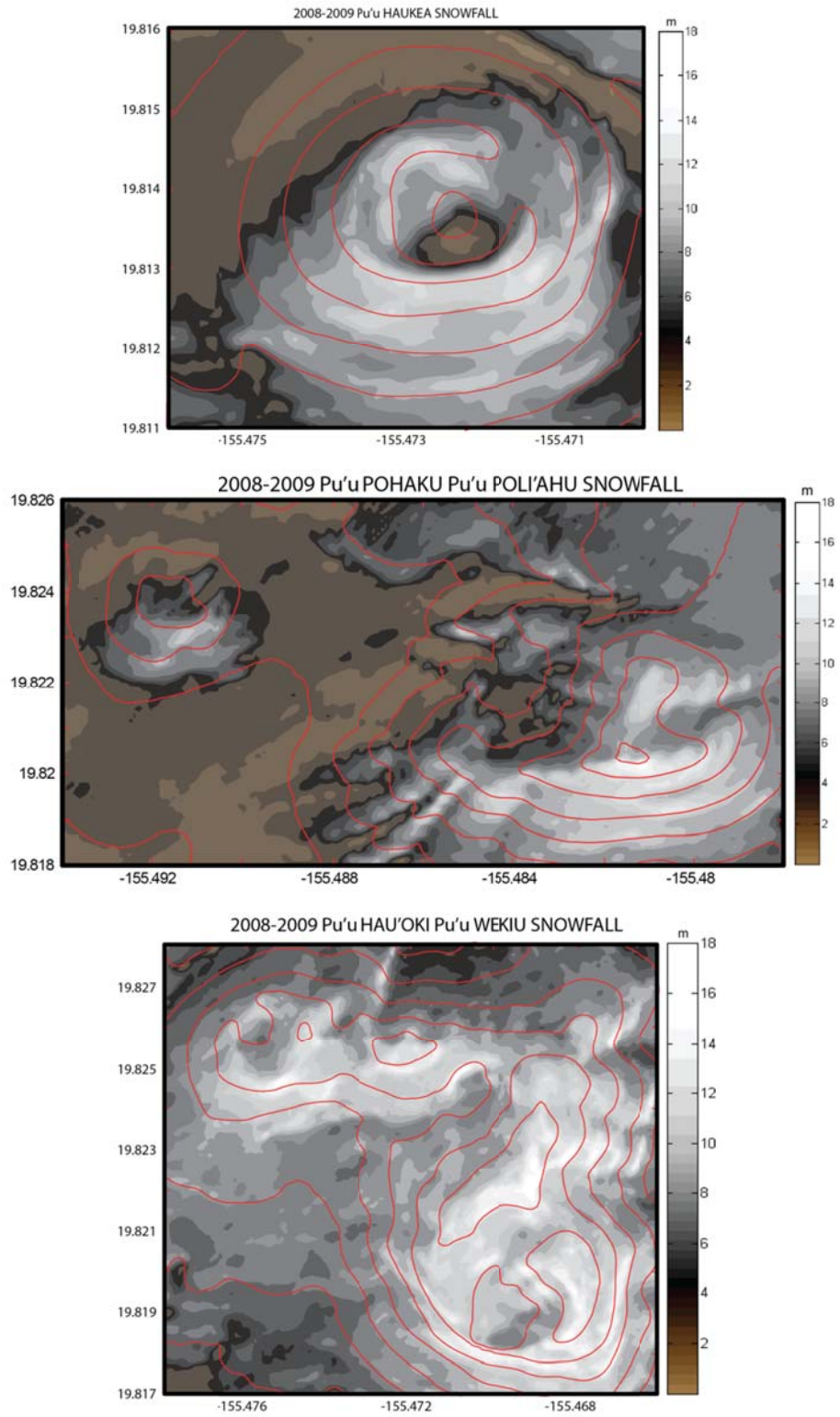


Fig 37: Same as Fig. 35 but for a) Pu'u Haukea; b) Pu'u Pōhaku and Pu'u Poli'ahu; and c) Pu'u Hau'oki and Pu'u Wēkiu

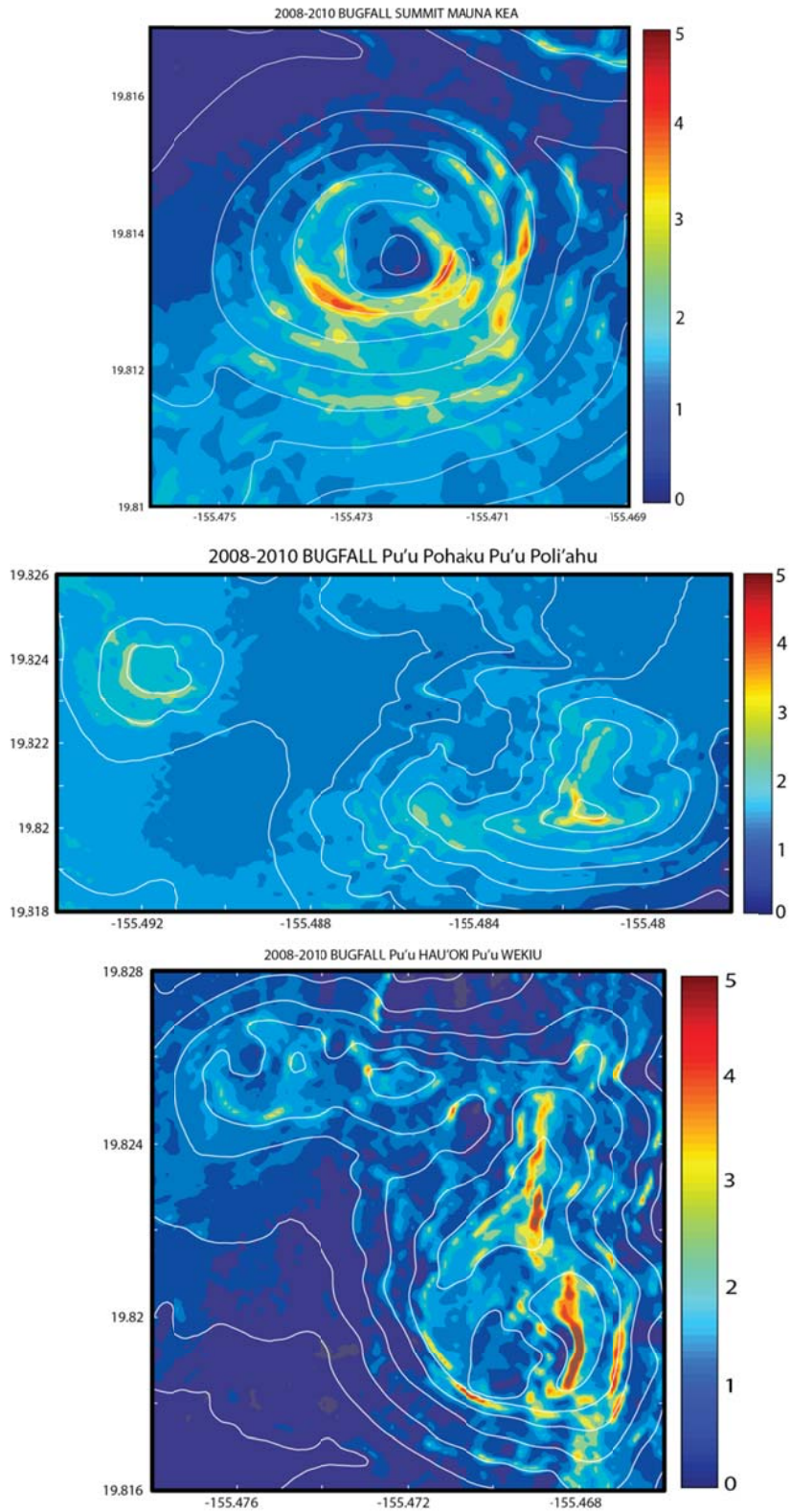


Fig 38: Same as Fig. 36 but for a) Pu'u Haukea; b) Pu'u Pōhaku and Pu'u Poli'ahu; and c) Pu'u Hau'oki and Pu'u Wēkiu

## References:

Anderson, E.A., 1976: A point energy and mass balance model of a snow cover. NOAA Technical Report NWS-19, 150 pp.

Ashlock, P. and W. Gagne, 1983: A remarkable new micropterous *Nysius* speices from the aeolian zone of Mauna Kea, Hawaii Island (Hemiptera: Lygaeidae). *International Journal of Entomology.*, **25.**, 47-55.

Barnes, S. L., 1973: Mesoscale objective analysis using weighted time-series observations. NOAA Tech Memo. ERL NSSL-62, National Severe Storms Laboratory, Norman, OK 73069, 60 pp. [NTIS-COM-73-10781].

Bely, P.-Y., 1987: Weather and Seeing on Mauna Kea. *Publications of the Astronomical Society of the Pacific.*, **99.**, 569-570.

Blumenstock, D.I. and S. Price, 1967: Climates of the States: Hawaii. *Climatology of the US*, No. 60-51. US Department of Commerce, 27 p.

Cao, G., T. W. Giambelluca, D. E. Stevens, and T. A. Schroeder, 2007: Inversion Variability in the Hawaiian Trade Wind Regime. *Journal of Climate.*, **20.**, 1145-1160.

Conant, S., 2007: Memorandum: Climate Variability and Microscale Ecology of Mauna Kea study. [Between Mauna Kea Management Board and Wēkiu Bug Scientific Advisory Committee].

da Silva, S. C., 2006: Climatological analysis of meteorological observations at the summit of Mauna Kea. Research, Dept. of Meteorology, University of Hawaii at Mānoa, 77 pp. [Available from Mauna Kea Weather Center website archives: [www.mkwc.ifa.hawaii.edu/archive/](http://www.mkwc.ifa.hawaii.edu/archive/)]

da Silva, S.C., 2011: High Altitude Climate Variability of the Island of Hawai'i. M.S. Thesis, Dept. of Meteorology, University of Hawaii at Mānoa. [Available from Dept. of Meteorology, University of Hawaii at Mānoa, 2525 Correa Rd., Honolulu, HI 96822.]

Eiben, J. and D. Rubinoff, 2010: Life history and captive rearing of the Wēkiu bug (*Nysius Wēkiuicola*, Lygaeidae), an alpine carnivore endemic to the Mauna Kea volcano of Hawaii. *Journal of Insect Conservation.*, **14.**, 701-709.

Englund, R.A., D.A. Polhemus, F.G. Howarth, and S.L. Montgomery, 2002: Range, habitat, and ecology of the Wēkiu Bug (*Nysius Wēkiuicola*), a rare insect species unique to Mauna Kea, Hawaii Island., Report prepared for Office of Mauna Kea Management, University of Hawaii at Hilo, 200 W. Kawili Street, Hilo, HI 96720.

-----, D.J. Preston, A. E. Vorsin, N. L. Evenhuis, S. Myers, and L.L. Englund, 2009: Results of the 2007-2008 Alien Arthropod Species and Wēkiu Bug Monitors on Mauna

Kea, Hawaii Island., Hawaii Biological Survey final report prepared for Office of Mauna Kea Management, University of Hawaii at Hilo, 200 W. Kawili Street, Hilo, HI 96720.

Ehse, J., 2007: GIS-based assessment of possible permafrost deposits on Mauna Kea, Hawaii using geographical climate modeling. M.A. Thesis, Department of Geography and Climate, Rheinisch-Westfälische Technische Hochschule University – Aachen, 106 pp.

Erasmus, D. A., 1986: Meteorological Conditions Affecting Observing Quality on Mauna Kea. *Publications of the Astronomical Society of the Pacific*, **98**, 254-259.

Fish and Wildlife Service, 2010: Endangered and Threatened Wildlife and Plants; Review of Native Species That are Candidates for Listing as Endangered or Threatened; Annual Notice of Findings on Resubmitted Petitions; Annual Description of Progress on Listing Action. 50 CFR Part 17 [Docket No. FWS-R9-ES-2010-0065;MO-9221050083-B2].

Greene, E.M., G.E. Liston, and R.A. Pielke, Sr., 1999: Simulation of above treeline snowdrift formation using a numerical snow-transport model. *Cold Regions Science and Technology*, **30**, 135-144.

Grinding, C. M., 1992: Temporal variability of the trade wind inversion: Measured with a boundary layer profiler. M.S. Thesis, Dept. of Meteorology, University of Hawaii at Mānoa, 93 pp. [Available from Dept. of Meteorology, University of Hawaii at Mānoa, 2525 Correa Rd., Honolulu, HI 96822.]

Group 70 International, 2000: Mauna Kea Science Reserve Master Plan: A final environmental impact statement Master Plan. Report prepared for Research Corporation of the University of Hawai'i by Group 70 International, 925 Bethel Street, 5<sup>th</sup> Floor. Honolulu, HI 96813.

Jackson, P.S. and J.C.R. Hunt, 1975: Turbulent wind flow over a low hill. *Quarterly Journal of the Royal Meteorological Society*, **101**, 929-955.

Kind, R.J., 1981: Snow Drifting. *Handbook of Snow, Principles, Processes, Management, and Use*. D.M. Gray and D.H. Male, Editors, Pergamon Press, 338-359.

Koch, S.E., M. DesJardins, and P.J. Kocin, 1983: An Interactive Barnes Objective Map Analysis Scheme for Use with Satellite and Conventional Data. *Journal of Climate and Applied Meteorology*, **22**, 1487-1503.

Kodama, K. R. and S. Businger, 1998: Weather and Forecasting challenges in the Pacific Region of the National Weather Service. *Weather and Forecasting*, **13**, 523-546.

Liston, G.E., 1995: Local Advection of Momentum, heat, and Moisture during the Melt of Patch Snow Covers, *Journal of Applied Meteorology*, **34**, 1705-1715.

- , and K. Elder, 2006a: A Meteorological Distribution System for High-Resolution Modeling (MicroMet). *Journal of Hydrometeorology*, **7**., 217-234..
- , and K. Elder, 2006b: A Distributed Snow-evolution Modeling System (SnowModel). *Journal of Hydrometeorology*., **7**., 1259 – 1276.
- , R.B. Haehnel, M. Sturm, C.A. Hiemstra, S. Berezovskaya, and R.D. Tabler, 1998: Instruments and Methods, Simulating complex snow distributions in windy environments using SnowTran-3D. *Journal of Glaciology*, **53**, 241-256.
- , and M. Sturm, 1998: A snow-transport model for complex terrain. *Journal of Glaciology*., **44**, 498-516.
- , and -----, 2002: Winter Precipitation Patterns in Arctic Alaska Determined from a Blowing Snow Model and Snow-Depth Observations. *Journal of Hydrometeorology*,**3**, 646-659.
- , and -----, 2006: A Meteorological Distribution System of High-Resolution Terrestrial Modeling (MicroMet). *Journal of hydrometeorology*, **7**, 217-234.
- , J.-G. Winther, O. Bruland, H. Elvehoy, K. Sand, and L. Karlof, 2000: Snow and blue-ice distribution patterns on the coastal Antarctic ice sheet. *Antarctic Science*., **12**, 69-79.
- Pomeroy, J.W., and D.M. Gray, 1990: Saltation of Snow. *Water Resources Research*, **26**, 1583-1594.
- Porter, S.C., 1997: Late Pleistocene Eolian Sediments Related to Pyroclastic Eruptions of Mauna Kea Volcano, Hawaii. *Quaternary Research*., **47**., 261-276.
- Prasad, R., D.G. Tarboton, G.E. Liston., C.H. Luce, and M.S. Seyfried, 2001: Testing a blowing snow model against distributed snow measurements at Upper Creek, Idaho, United States of America. *Water Resources Research*, **37**, 1341-1350.
- Swan, L., 1963: Aeolian Zone. *Science*., **140**., 77-78.
- Schmidt, R.A, 1982: Vertical Profiles of Wind Speed, Snow Concentration, and Humidity in Blowing Snow. *Boundary Layer Meteorology*.,**23**, 223-246.
- Sustainable Resources Group International, Inc., 2009: Natural Resources Management Plan for the UH Management Areas on Mauna Kea: A sub-plan of the Mauna Kea Comprehensive Management Plan. Prepared by the Sustainable Resources Group Internationals, Inc.,111 Hekili Street, Suite A373, Kailua, HI, 98734.
- Ugolini, F. C., 1974: Hydrothermal origins of the clays from the upper slopes of Mauna Kea, Hawaii. *Clay and Clay Minerals*, **22**., 189-194.

Whiteman, C.D., 2000: Mountain Meteorology – Fundamentals and Applications. New York: Oxford University Press.

Wiggs, G.F.S., J.E. Bullard, B. Garvey, and I. Castro, 2002: Interactions between airflow and valey topography with implications for aeolian sediment transport. *Physical Geography*, **23.**, 366-380.

Wolfe, E.W., W.S. Wise, and G.B. Dalrymple, 1997: The geology and petrology of Mauna Kea Volcano, Hawaii – A Study of Post Shield Volcanism. *U.S. Geological Survey Professional Paper*, **1557.**, pp. 143.

Worthley, L. E., 1967: Weather phenomena in Hawaii. Part 1. Synoptic climatology of Hawaii. Hawaii Institute of Geophysics, University of Hawaii, 40 pp. [Available from Dept. of Meteorology, University of Hawaii, 2525 Correa Rd., Honolulu, HI 96822.]